УДК550.837.211: 477 DOI: https://doi.org/10.24028/gj.v45i2.278306

Geoelectric model of the Earth's crust and upper mantle of the Dniester-Bug megablock of the Ukrainian Shield

I.M. Logvinov, I.V. Gordienko, V.N. Tarasov, A.N. Logvinova, 2023

S.I. Subbotin Institute of Geophysics of the National Academy of Sciences of Ukraine, Kyiv, Ukraine

Received 13 December 2022

A network of long-period magnetotelluric and magnetovariational data (124 sites) in the period range of 9—16 to 2500—6400 s made it possible to explore the geoelectric structure of the Erth's crust and upper mantle of most of the Dniester-Bug and adjacent megablocks of the Ukrainian shield. Based on the resistivity cross-sections along the profiles (with 2D inversion), a three-dimensional matrix was created for the territory limited by coordinates 27.7—30.4° E and 47.7—49.4° N, which included the spatial coordinates of each grid node on each profile, the power of the model cells, and the resistance value in the cell. As a result, geoelectrical anomalous structures were identified at different depths from 3 to 100 km.

The entire block of rocks 200×200 km down to a depth of 100 km is characterized by high resistivity, against which objects of reduced resistivity (LRO) are identified.

The resulting distribution of high-resistivity rocks over the entire depth of the model is in good agreement with the laboratory dependencies obtained both for the rocks of the Ukrainian Shield and other data. Model data show a significant difference in resistivities in the upper 14—16 km (above 10^5 Ohm), lower crust (about 10^4 Ohm), and upper mantle (10^3 Ohm). Against a general decrease in resistance with depth in the Earth's crust, three regions were identified in which anomalously high (for a given depth) resistances extend to the entire thickness of the crust. These high-resistivity objects are consistent with positive Bouguer anomalies.

Against the background of high-resistivity rocks, LROs stand out, the resistance of which does not exceed 120 Ohm·m. The spatial dimensions of the LRO zones indicate their locality and do not form a continuous layer. An analysis of the distribution of LROs in space and depth suggests a genetic relationship between mantle LROs and crustal LROs. Comparison of mantle LROs with the Beltska zone of modern activation on the territory of Ukraine shows their good agreement both vertically and horizontally. To explain the lower LRO resistivity in the upper mantle, overheating of the rocks to solidus and 2—3 % melting and/or the presence of fluids is necessary [Gordienko, 2017]. In recent studies discussing the influence of thermobaric conditions and the fluid content necessary to explain the presence of increased conductivity in the upper mantle, the authors of [Blatter et al., 2022] concluded that an anomalously large amount of volatiles is needed with small amounts of melt. The assumption that mantle LROs are related to crustal LROs has been tested by comparing LROs with fault zones.

The presence of LROs in the mantle, their vertical extent, and their connection with rejuvenated fault systems can serve as a basis for the deep migration of fluids enriched in volatiles.

Key words: Earth's crust and upper mantle, Ukrainian Shield, electrical conductivity.

Citation: *Logvinov, I.M., Gordienko, I.V., Tarasov, V.N., & Logvinova, A.N.* (2023). Geoelectric model of the Earth's crust and upper mantle of the Dniester-Bug megablock of the Ukrainian Shield. *Geofizicheskiy Zhurnal*, *45*(2), 3—29. https://doi.org/10.24028/gj.v45i2.278306.

Introduction. The work is devoted to the study of the geoelectric structure of the Earth's crust and upper mantle of the southern part of the Dniester-Bug megablock of the Ukrainian Shield (USh) [Shcherbak, Bobrov, 2006] (Fig. 1). Judging by the map of the erosion cut of the shield (see Fig. 1, *a*), the maximum cut depths for the shield are distributed over a larger area of the megablock (up to 30 km against the background of depths of 17±5 km for most of the shield) [Gordienko et al., 2005]. Numerous deposits of various minerals (polymetals, graphite, etc.) with an electronic type of conductivity (polymetals, noble metals, etc.) are known on the territory of the megablock, the formation of which is due to Precambrian and Cimmerian activization [Shcherbak, Bobrov, 2006; Shumlyanskiy, 2007], the study area is located in the western part of the Central graphite-bearing area [Yatsenko, 1998]. These minerals are characterized by values of reduced resistance, which differ sharply from high-resistivity host crystalline rocks. The territory is intersected by regional faults of different ages [Verkhovtsev, 2008; Verkhovtsev et al., 2012; Entin, 2005, etc.].

The Dniester-Bug megablock has been covered by numerous geophysical studies. A number of international profiles of deep seismic sounding (DSS) pass along the edges of the territory [Kharitonov et al., 1995; Sollogub, 1986; Ilchenko, 2002] (see Fig. 1). According to the DSS data on the geotraverse YI, V.B. Sollogub

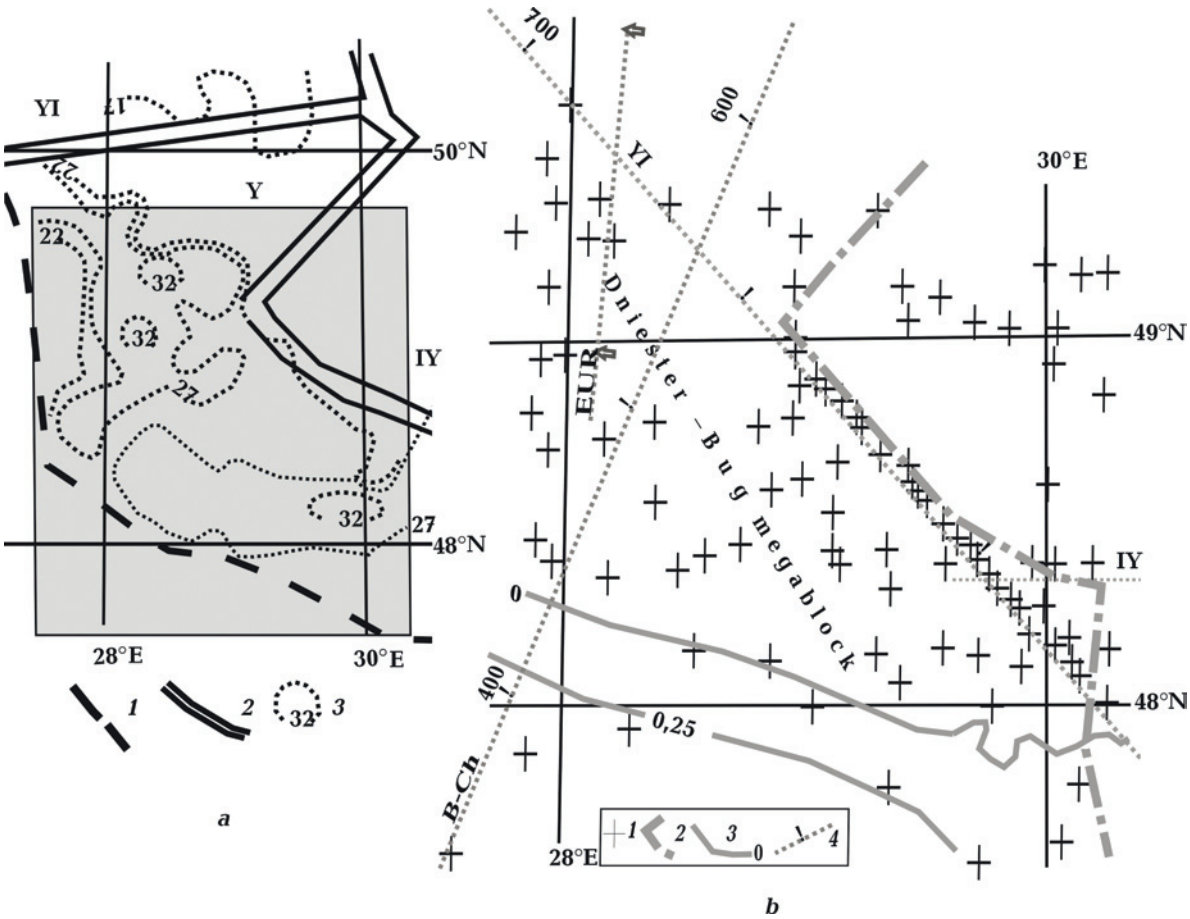

Fig. 1. Location of the studied area (gray rectangle) (*a*): *1* — contour Ukrainian Shield; *2* — megablock boundaries (roman numerals): YI — Volyn, Y — Dnister-Bug, IY — Ros-Tikich [Shcherbak, Bobrov, 2006]; *3* — erosion cut depth in km [Gordienko et al., 2005]. Studied area (*b*): *1* — location of MT observation sites; *2* — boundary of the Dniester-Bug megablock [Shcherbak, Bobrov, 2006]; *3* — thickness (in m) of the pre-Riphean sediments [National ..., 2007]; *4* — seismic profiles (arrow — pickets): EUR — Eurobridge [Ilchenko, 2002], B-Ch — Bucharest—Chornobyl [Kharitonov et al., 1995].

[Sollogub, 1988], identified a belt of an increased crustal thickness (Odesa-Vinnytsia zone) against the background of crustal thickness of 40—45 km, where the depth of the Moho (M) boundary reaches 60 km. Several positive Bouguer anomalies have been identified in the gravitational field [National…, 2007]. The magnetic model of the Earth's crust notes that «The Podolsk block is characterized by the largest and most intense isometric and elongated magnetic bodies» [Orlyuk, 2000]. Magnetic anomalies with an intensity of 2—6 A/m were identified by V.V. Gordienko in the range of 15—42 km in the northern and southeastern parts of the study area [Gordienko et al., 2005]. The southern part of the study region is located within an area with anomalously high heat flow (HF) values [Gordienko, 2012], which are accompanied by uplifts in the Late Pliocene—Quaternary [Verkhovtsev, 2008; Verkhovtsev et al., 2012].

Given such a large amount of information, questions about a connection between known geological and geophysical data and geoelectric parameters are of interest. Some, while preliminary, answers can be obtained based on the results of studies using variations of the magnetotelluric (MT) field.

A dense network of MT data collected over the past 50 years made it possible to reveal electrically conductive structures on the territory of the USh. The bulk of the research results was obtained by the production organizations of the Ministry of Geology of the Ukrainian SSR (MinGeo) in the last century under the leadership of A.I. Ingerov and V.I. Tregubenko. A detailed analysis of the results of these studies is given in [Gordienko et al., 2005; Logvinov, 2015; Logvinov, Tarasov, 2019]. In these works, based on the processing of areal magnetotelluric studies, magnetotelluric sounding (MTS) curves and, in part, induction vectors are presented. Thanks to these works, the geoelectric structure of near-surface rocks of the Ukrainian shield is quite fully represented. However, many questions remain related to the structure of the entire thickness of the Earth's crust and upper mantle. These issues have not been resolved by these studies, because the geoelectric parameters of the subsurface were obtained using only qualitative interpretation methods.

Using a 2D interpretation (direct problem) of the MTS amplitude curves (ρ_k curves) and Wiese vectors in the southwestern part of the region, Burakhovich et al. [1997] identified a conductive object in the upper mantle that is spatially consistent with the Beltska anomaly of high HF values.

In the previous works of the authors for the entire territory of USh to the west of 30° E based on results of MT studies at several hundred sites, the geoelectric parameters of the Earth's crust and upper mantle were estimated using one-dimensional (1D) and two-dimensional (2D) inversions [Gordienko et al., 2005; Logvinov, Tarasov, 2019]. 3D inversion program using a thin layer model, the areal distribution of conductivity in the upper part of the Earth's crust in the northwestern part of USh was analyzed [Kovachikova et al., 2022]. On the basis of these studies, numerous objects of low (ρ less than 100 Ohm·m) resistivity were found in the Earth's crust. Some of these objects are in good agreement with the nodes of the concentration of deposits of ore minerals.

Results of MT studies. ***Experimental data.*** The bulk of the results of magnetotelluric studies of the region was obtained by the production organizations of the MinGeo under the leadership of A.I. Ingerov and V.I. Tregubenko. These results are presented in the form of MTS curves (apparent resistivity and impedance phases) in the range from 1—20 to 900—1000 s, at individual points in the range of periods from 1—20 to 4000—8000 s. Most points lack magnetovariational interpretation parameters. All the indicated parameters of the experimental data were considered in the inversion.

From the end of the 20th century, research in MT was carried out by employees of the Institute of Geophysics of the National Academy of Sciences of Ukraine (IGF). The first works were carried out on the southward extension of the Eurobridge international profile [Burakhovich et al., 1997]. Analog records of the MT field obtained on photo paper were digitized by us and processed us-

ing modern programs, and the parameters of the impedance matrix and vertical magnetic transition function (VMTF) were obtained in the range of periods 10—6400 s [Gordienko et al., 2005]. Subsequently, the staff of the IGF tectonosphere department made observations of the MT field with modern digital equipment at several points in the southern part of the territory [Gordienko et al., 2005]. In 2020 and 2021, the employees of the IGF tectonosphere department carried out MT observations and determined the interpretation parameters of apparent resistivity and impedance phases of MTS curves and VMMF curves in the range of periods from 10—20 to 6000—10000 s. Processing of digital records of MT field variations was carried out using two software packages [Ladanivskiy, 2003; Varentsov, 2007].

Based on the results of all studies, a database of experimental data was compiled, which included the MTS and VMTF curves at 124 points (see Fig. 1, *b*).

2D inversion. First, the experimental data were interpreted using the 2D REBOCC inverse modeling procedure along individual profiles crossing the area [Siripunvaraporn, Egbert, 2000]. In the modeling procedure, MTS and VMTF data were used. The values of the MT sounding curves performed by prospecting organizations are estimated with an accuracygenerally not exceeding 15 % in amplitude and 3—5° in phase. The results of modern processing of MT field variations are presented with the definition of the error of each interpretive parameter over the entire interval of periods. Since most of the data used in modeling were obtained by exploration organizations, we adopted errors proportional to the triple error in determining each modeling parameter in the REBOCC procedure: 0.1 for the VMTF, 10 % for the impedance phase, and 30 % for the apparent resistivity. Previous studies have revealed the presence of low-resistivity structures with different strikes. Since the MTS curves provided by prospecting organizations were presented only for azimuths 0° and 90°, the interpretation profiles were arranged in the latitudinal and meridional directions.

Modeling was performed along 11 profiles (Fig. 2, 3); the minimum length of 100 km was determined by the presence of points falling into the profile belt with a width of about 10—15 km. When choosing points suitable for modeling, the following conditions were met: according to the applied procedure described in detail [Logvinov, 2015], the choice of MTS curves was conditioned by the availability of impedance phases. The number of interpretation parameters for each TE, TM, and TP mode was at least 75 % of the used frequency range.

The horizontal step varied from 3 to 10 km following the density of observation points on the profile. The step along the vertical axis for all profiles was 100—500 m for the upper 2 km and 1000—4000 m for the depth interval of 2—50 km. Below, the step varied from 8 to 30 km. Geoelectric sections are built to a depth of 50 to 110 km, depending on the used frequency range and the length of the modeling profile. At the same time, for the conditional determination of parameters at depths less than 2—3 km, the level of values of the longitudinal resistance of the sedimentary rocks of the USh requires the presence of interpretive parameters at periods of less than 1—4 s. Therefore, the geoelectric parameters down to a depth of 2 km were fixed in the inversion.

When compiling the initial interpretative model on all profiles, a priori geological and geophysical information on the structure of the region was used. The geoelectric parameters of the mantle in the starting models were taken according to the 1D inversion of the induction curve at the Kyiv geomagnetic observatory [Ladanivskiy et al., 2019]. Considering the results of 1D inversion in obs. Kyiv and at points on the USh, the following parameters of the host environment («normal» section) are accepted:

- from the Earth's surface to a depth of 30 km, the value of resistivity (ρ) is assumed to be 1000 Ohm·m;
- from 30 to 50 km — 700 Ohm·m;
- from 50 to 160 km — 400 Ohm·m;
- from 160 to 240 km — 100 Ohm·m;
- from 240 to 390 km — 65 Ohm·m;

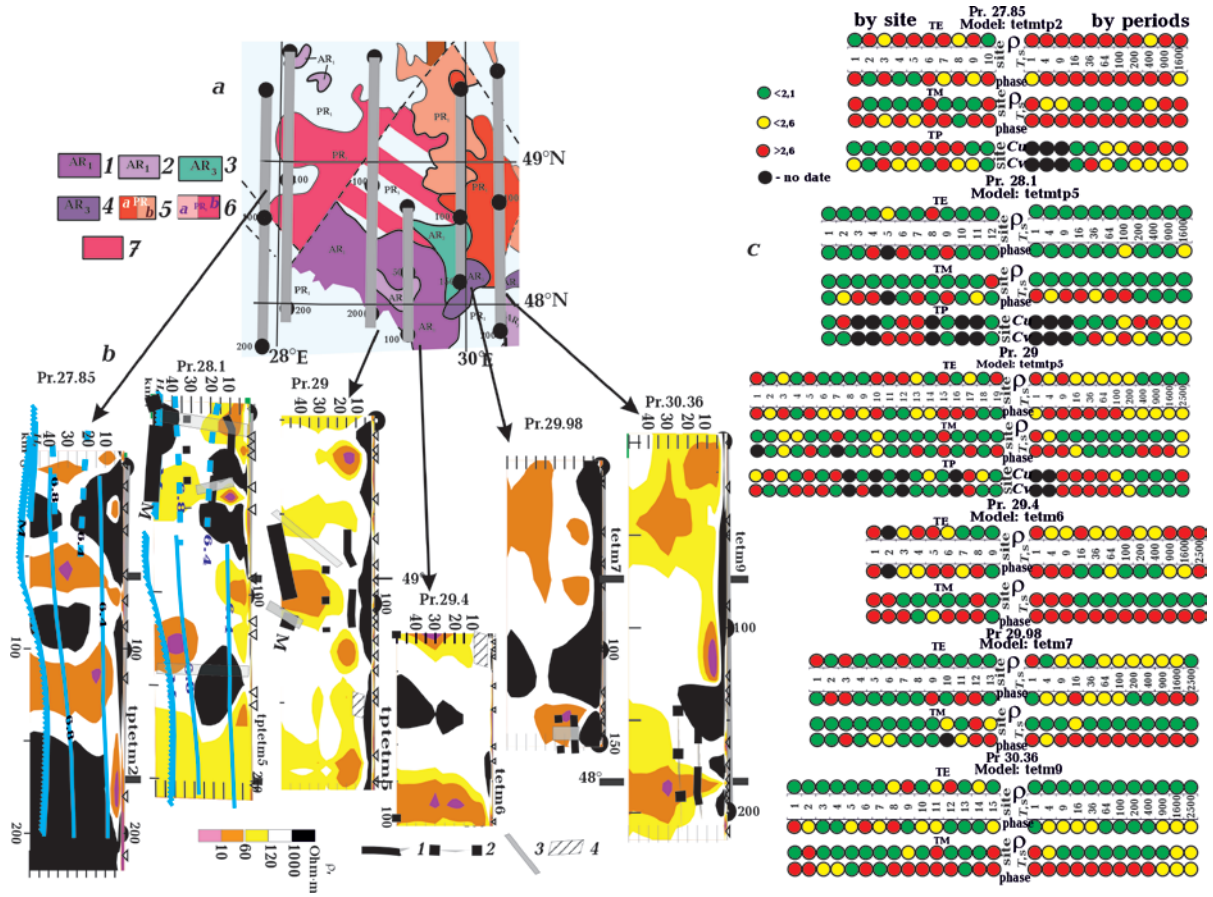

Fig. 2. Geological map of pre-Riphean deposits [National…, 2007] (*a*): *1* — enderbites; *2* — gneisses, crystalline schists, amphibolites, calciphyres, ferruginous quartzites, mafic rocks, ultramafic rocks; *3* — plagiogranites, diorites, granodiarites, gneisses, amphibolites; *4* — gneisses, ferruginous quartzites, marbles, crystalline schists, gvbbro, periditites, pyroxenites; *5* — granites (*a*), migmatites (*b*); *6* — granites, migmatites (*a*), charnockites (*b*); *7* — granites, migmatites, granodiorites, diorites. Geoelectric models along meridional profiles with the best RMS. Seismogeological sections along geotraverses EUROBRIDGE (dashed line); Bucharest—Chornobyl (solid) and YI (see Fig. 1) (*b*): *1*, *2* — velocity contours: V_P =6.4 km/s (*1*), V_P = 6.8 km/s (*2*), *3* — fault lines; *4* — low velocity zones. Residuals (RMS) in experimental and model data (*c*).

– from 390 to 520 km — 40 Ohm·m;
– from 520 to 650 km — 5 Ohm·m.

When creating starting models, the thickness of sedimentary deposits on the territory of Ukraine was taken from the map «Isohypses of the surface of the pre-Riphean basement» [National…, 2007]. The inversion program for correct calculations requires setting geoelectric parameters at a distance of several hundred kilometers in both directions from the observation points on the profile. At the western ends of the latitudinal profiles, the geoelectric parameters of sedimentary rocks were specified in the models based on the total longitudinal conductivity of the sediments (Ssd) of the Volyn-Podolsk Plate and the Carpathian Foredeep [Logvinov, 2015]; the eastern parts of the profiles pass through the territory of the USh, where the Ssd values do not exceed 10 S [Tregubenko et al., 1989]. At the southern ends of the meridional profiles, the geoelectric parameters of sedimentary rocks were set in the models based on the Ssd of the territories of Moldova and Romania (up to the Fokshan depression) [Shilova, Bilinskiy, 1983; Stănică et al., 1999; Scientific…, 2013]; the northern parts of the profiles pass through the territory of the Ukrainian Shield, where the Ssd values do not exceed 10 S [Tregubenko et al., 1989].

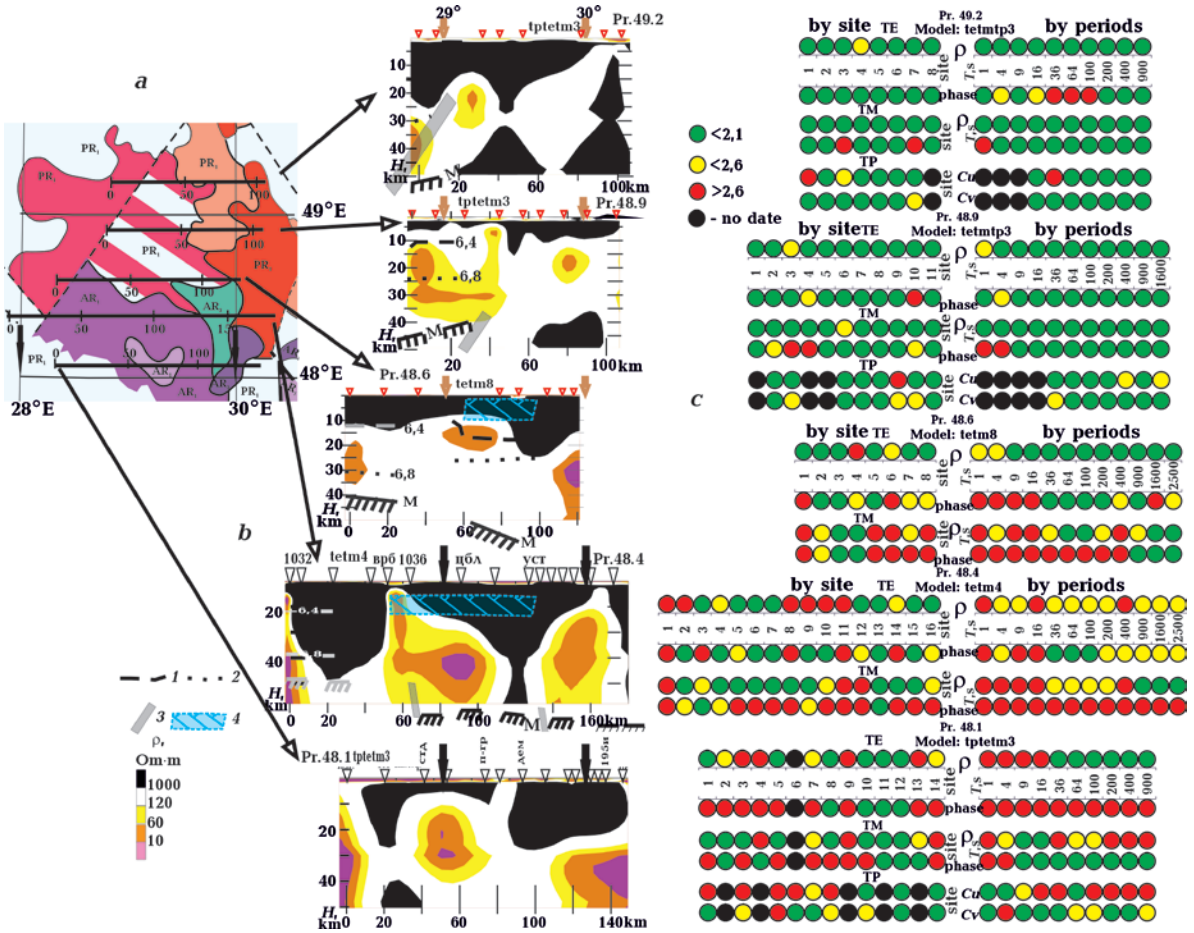

Fig. 3. Geological map of pre-Riphean deposits [National…, 2007] (*a*). Geoelectric models along latitudinal profiles with the best RMS. Seismogeological sections along geotraverses (see Fig. 1) Bucharest-Chornobyl, IY, YI (*b*). Residuals (RMS) in experimental and model data (*c*). See symbols in Fig. 2.

Methodically, the modeling was carried out in three stages. To start with, we selected the models satisfying the induction mode — separately for the longitudinal MTS curves (TE mode) and the VMTF components (TP mode). Secondly, the selection was carried out using the TE and TP modes and the TP and TE modes. At this stage, the inversion was carried out with the choice, as a start, of the model that was obtained with the minimum RMS (the gradation of residuals) for the TE and TP modes, respectively. The second stage ended with a choice of two approaches of models with the smallest values of RMS by periods and by points. Thirdly, models were selectedthat satisfied the TE and TM modes (longitudinal and transverse MTS curves, respectively) and the TM mode and TP-TE-TM modes, taking into account the results obtained at the previous stage. At the final stage, the obtained results were compared and the model with the lowest RMS values for the TE and TP modes was selected.

Below are the modeling results for profiles, the names of which correspond to the coordinate of the middle line of the profile strip. The margin of RMS is made taking into account their values that satisfy the representation of the model in the form of a two-dimensional environment: up to values of 2.1 are completely satisfactory, the interval 2.1—2.6 is partially satisfactory, more than 2.6 is completely unsatisfactory, and the black is no data. When constructing sections and volumetric models, the TAR 3D program developed by the authors [Tarasov et al., 2013] was used, which makes it possible to visualize 2D geoelectric results based on modeling data.

Let's start with the meridional profiles, on which it is possible to identify conductive objects of a quasi-latitudinal strike. In the band from 27.8° E to 30.4° E, modeling was carried out along four profiles with a length of pr27.85 and pr29.4 — 150 km, pr28.1 — 170 km, pr29.98 — 100 km (see Fig. 2). Ten points fell into the 27.85 profile band; 12 points fell into the 28.1 profile band. On both profiles, data were used in the interval of periods 1—1600 s. On pr27.8 and pr29, the number of interpretative parameters made it possible to use all three modes for inversions; on the remaining profiles, the amount of data for the TP mode is less than 70 %, and therefore the inversion was carried out using only the TE and TM modes. The distance between the points made it possible to carry out modeling at a step between the points of 6—8 km on pr27.85 and 4—9 km on pr28.1. Nineteen points fell into the strip pr29, pr29.4 — 9, pr29.98 — 9, and pr30.36 — 15 points (see Fig. 2, *b*). On the listed profiles, data were used in the interval of periods of 1—2500 s. The distance between the points made it possible to carry out modeling at a step between the points of 4—7 km on pr29, 4—8 km on pr29.4 and 30.38, and 3—6 km on pr29.98.

Corresponding to such a step between points, low-resistivity objects (LRO) in the upper crust with horizontal dimensions less than 10 km cannot be identified reliably. The most reliable results were obtained for profiles where all three modes were used for inversion. When analyzing the spatial dimensions of the LRO, it is necessary to consider the correctness of the isoclines due to the use of the SURFER program. Therefore, the LRO allocated for 1—2 points (distanced at a distance of 15—20 km from neighboring ones) have overestimated width values in the figures. These sites include LRO in the districts: pk110 pr27.85, pk130 pr28.1, pk90 pr29.4, and pk20 r29.98.

The distribution of RMS of all modes of the model for pr27.85 (see Fig. 2, *c*) mainly exceeds 2.4, which indicates poor compliance of the model as a whole with the idea of a two-dimensional medium, although in some sections of the profile, the RMS for the TE and TP modes are about 2. For pr28.1 and 29, RMS for all modes mainly do not exceed 2.4, which indicates a good agreement between the selected conductors of the two-dimensional model. Although the distance between these profiles is about 50 km, the position of the LRO in space is close. Therefore, the LRO identified on these profiles can be assumed to extend up to pr27.85. Changes in the depth of the centers and other geoelectric parameters of the identified LRO on different profiles can be caused by the number and location of observation points and by the actual state of the region's subsoil. The latter assumption can be confirmed by the change in the geoelectric parameters of the LRO identified on all profiles in their southern part. For pr29.4 (see Fig. 2, *c*), the distribution of RMS of all model modes mainly exceeds 2.4, which indicates poor compliance of the model as a whole with the idea of a two-dimensional medium. On pr29.98 and 30.36 located to the east, the RMS values for all modes do not exceed 2.4, which indicates a good agreement between the selected conductors and the two-dimensional model. On all these profiles, large values of RMS are primarily due to the poor quality of the phases of the TM mode impedances.

On all profiles, the maximum number of local LROs (with small differences in size, width, and depth) is identified in the granite layer. Attention is drawn to the almost complete absence of local LRO in the intermediate layer. On all profiles, 1—2 LROs are identified, which stretch in narrow zones from upper mantle depths to transitional or granite layers.

Conventionally, it is possible to distinguish several latitudinal zones throughout the studied territory, in which LROs of various spatial sizes have been identified on several profiles. On the western profiles, up to pr29, about four zones with transverse dimensions of about 20 km can be distinguished. At pr29.98 and pr30.36, the transverse dimensions of the LRO increase to approximately 50 km, and the zones identified on the previous profiles seem to merge into two — in the south to 48.5° N and north to 48.5° N.

Latitudinal profiles (on which conducting objects of quasi-meridional strike can be dis-

tinguished) are distinguished by many points but shorter than the meridional profiles (see Fig. 3).

Two profiles (48.9 and 49.2) start approximately from 29° E; pr48.6, 48.4, and 48.1 start from approximately 28° E and have a length of more than 100 km (see Fig. 3, *a*). To the strip of pr48.1 fell into 14, pr48.4 — 16, pr48.6 — 8, pr48.9 —11, and pr.49.2 — 8 points. The data of all three modes were used on pr48.1 in the interval of periods 9—2500 s, pr48.9 in the interval of periods 1—1600 s, on pr49.2 in the interval of periods 4—1600 s. On profiles 48.4 and 48.6, the amount of data for the TP mode is less than 70 %, and therefore the inversion was carried out using only the TE and TM modes in the interval of periods 1—2500 s. The distance between the points made it possible to carry out modeling with a step between the points of 3—4 km on pr48.1, 3—7 km on pr49.4 and 49.6, 3 km on pr48.9, and 3—6 km on pr49.2.

On pr48.6, 48.9, and 49.2, the RMS values for all modes mainly do not exceed 2.4, which indicates a good agreement between the conductors identified here and the two-dimensional model. For the profiles located to the south (see Fig. 3, *a*), the distribution of RMS for the phases of the TE and TM modes of the model mainly exceeds 2.4. On the one hand, this is due to poor processing quality of the past studies.

On all profiles, LROs of different spatial sizes were found in the region of 29°E (see Fig. 3, *b*). The centers of the most conductive parts at pr48.1 and 48.4 are located in the basalt layer, moving northwards into the transition layer. The second LRO zone (located in the region of 30° E) is distinguished on all profiles except for pr49.2. On profiles from 48.1 to 48.6, the most conductive parts are located at the boundary of the transitional and basaltic layers; on pr48.9, the LRO sharply decreases in size and is located only in the transitional layer.

On the latitudinal profiles on all models, the rocks with the ρ value of hundreds and thousands of Ohmmeters have the largest volume. On all profiles, LROs of different spatial sizes were found in the region of 29° E. (see Fig. 3, *b*). The centers of the most conductive parts at pr48.1 and 48.4 are located in the basalt, moving northwards into the transition layer. The second LRO zone (located in the region of 30° E) is distinguished on all profiles except for pr49.2. On profiles from 48.1 to 48.6, the most conductive parts are located at the boundary of the transitional and basaltic layers, on ex. 48.9, the LRO sharply decreases in size and is located only in the transitional layer.

The geoelectric sections (see Fig. 2, *b*, 3, *b*) show the distribution of V_P velocities in the seismic sections of the geoelectric profiles along the geotraverses: EUROBRIDGE-97 [Ilchenko, 2002], Bucharest-Chornobyl [Kharitonov et al., 1995], YI [Sollogub, 1988] and IY [Sollogub et al., 1978] (see Fig. 1).

A clear connection between the LRO and the undulations of the M surface is not observed on all meridional profiles. However, on the western profiles in the range of 48.5—49° N, it is planned to coordinate the position of the LRO with the rise of M (see Fig. 2, *b*). It can be conditionally assumed that the zones of deep occurrence of M (pr29.98 and 30.36) correspond to LRO, the most conductive parts of which are located above 30 km. Most of the faults shown on the seismic sections, which are intersected by geoelectric profiles, are consistent with the location of the LRO. On pr29.4, the LRO is located under the zone of low velocities identified on the IY geotraverse [Sollogub et al., 1978].

On the northern latitudinal profiles (pr48.6-49.2), it can be assumed that the LRO is related to the uplift of the M surface, while such a relationship is not observed on the other profiles (see Fig. 3, *b*). Where fault zones are identified on seismic sections, the connection with the LRO is obvious. On all profiles, the LROs accompany the fault zones along the entire length of the faults to a depth consistent with the depth of the upper edges of the fault zones (see Fig. 2, *b*, 3, *b*). As well as on the meridional profiles, the zones of low velocities identified on geotraverses IY [Sollogub et al., 1978] and YI [Sollogub et al., 1988] are accompanied by LRO, the top of which is below these zones.

Volumetric geoelectric model. Based on the resistivity cross-sections along the profiles, a three-dimensional matrix was created that included the spatial coordinates of each grid node on each profile, the model cells' thickness, and the cell's resistivity. Taking into account the density of modeling profiles, it is possible to take the scale of the resulting resistivity map for the area from 27.7° to 30.4° E and from 47.4° to 49.4° N equal to 1:2 000 000.

Before analyzing volumetric geoelectric models, one has to broadly define the horizontal parameters of identified geoelectric objects (layers and local objects). The general concept of a layer in geology has many definitions. The most general definition of a layer can be found in [Rika, Malyshevskiy, 1989] «… a flat or curved body of rocks *with a relatively small thickness and disproportionately large dimensions along strike and dip*» (our italics).

Theoretically, the process of field propagation in a conductor is described by the diffusion equation, the only justified characteristic of which is the field diffusion depth (the field penetration depth into the medium at which the field decays by a factor of e=2.71). In practice, in MT studies, the field penetration depth (δ) of a plane wave in a homogeneous conducting medium is defined as $\delta=503(\rho T)^{1/2}$ (m), where ρ is the resistivity of the conductor material (Ohm·m), T is the field variation period in seconds. The wavelength for the same depth is defined as $\lambda=2\pi\delta$. Geoelectric objects with horizontal dimensions commensurate with the wavelength in the conductive object and thickness several times smaller than the horizontal dimensions will be called a conductive layer, and those that do not satisfy the specified parameters — LRO.

By definition, the resistance of a homogeneous conductor with a constant cross-section depends on the properties of the conductor's substance, length, and cross-section. According to Pouillet's law, resistance (R) is calculated by the formula: $R=\rho(l/Q)$, where ρ is the resistivity of the conductor material, in Ohm·m, l is the length of the conductor (in m), $Q=d\times h$ (d is width, h is thickness) is the cross-sectional area (in m^2). Accordingly, the conductivity of the conductor (G) will be $G=Q/\rho l$. In the case of an object that is inhomogeneous in conductivity, its integral conductivity will be equal to the sum of connected conducting blocks with different values $\rho_i - G_{sum}=\sum(Q_i/\rho_i l_i)$. For a homogeneous space or a horizontally layered medium in MT studies, the concept of the total longitudinal conductivity of the layer ($S=h/\rho$) was introduced, from which it follows that a layer is understood as an object whose length and width are commensurate.

The determination of objects geoelectric parameters is done using the results of REBOCC modeling. A feature of the program is the approach when the model cannot contain sharp boundaries, and the distribution of conducting objects with the lowest possible resistance values is sought. Therefore, it can be assumed that the largest contribution to the values of the integrated conductivity of local LROs will be from objects with ρ less than 40 Ohm·m (with an equal volume of blocks of objects with a resistance of less than 120 Ohm·m).

It is known that MT methods have a poor resolution concerning high-resistance rocks; therefore, the change in high values of ρ is reflected in the sections of three-dimensional models (Fig. 4) by values of more than 1000 Ohm·m (we will designate areas with a resistance of more than 4000 Ohm·m as high-resistance objects (HROs)), which helps to compare the distributions of ρ in the model with those for crystalline rocks obtained in laboratory studies. The least reliable constructions refer to the part of the territory between 47.8 and 49.2° N in the interval 28.3—28.7° E. There are few experimental data in this region, and the available ones are characterized by MTS curves in a reduced range of periods and the absence of impedance phases. Therefore, for high-resistivity rocks, the wavelength in which already at depths of more than 3 km is more than 20 km (which is commensurate with the distance between the modeling profiles), it is possible to build the HRO distribution using interpolation over all points of the territory. To analyze the distribution of objects with ρ<100 **Ohm·m, conditional interpola**tion for the entire study area can be used for

depths of more than 20—30 km. Therefore, the distribution of resistances is analyzed for two regions: the western (in the interval of longitudes 27.7—28.3°) and the eastern (in the interval of longitudes 28.7—30.4°).

To analyze the most general characteristics of geoelectric parameters throughout the study area, several types of drawings were constructed. The construction of 3D models was carried out using the TAR3D program, created in the Matlab environment by the authors of the article [Tarasov et al., 2013]. Data interpolation was carried out by the Delaunay method.

From the constructed volumetric models for the depth interval of 3—100 km (see Fig. 4), it can be seen that the main volume of rocks in the territory for the entire thickness from 3 to 100 km has a resistivity much higher than 1000 Ohm·m. The Earth's crust and upper mantle of the region under consideration with horizontal dimensions of about 200×200 km, whose resistivity matrix contains 20330 values (see Fig. 4), is a block of high-resistivity rocks that form the host environment. Each depth slice has 700 points of ρ determinations, of which 530—670 points have resistance values above 200 Ohm·m. Up to 10—15 km, high-resistivity rocks with ρ>1000 Ohm·m form an almost continuous massif, in the central part of which rocks with ρ values reaching 10000 Ohm·m occupy most of the rock volume (see Fig. 4, *c*). Below 15 km, the area of rocks with ρ>4000 Ohm·m is significantly reduced, and deeper than 25 km up to the base of the Earth's crust, rocks with ρ>4000 Ohm·m

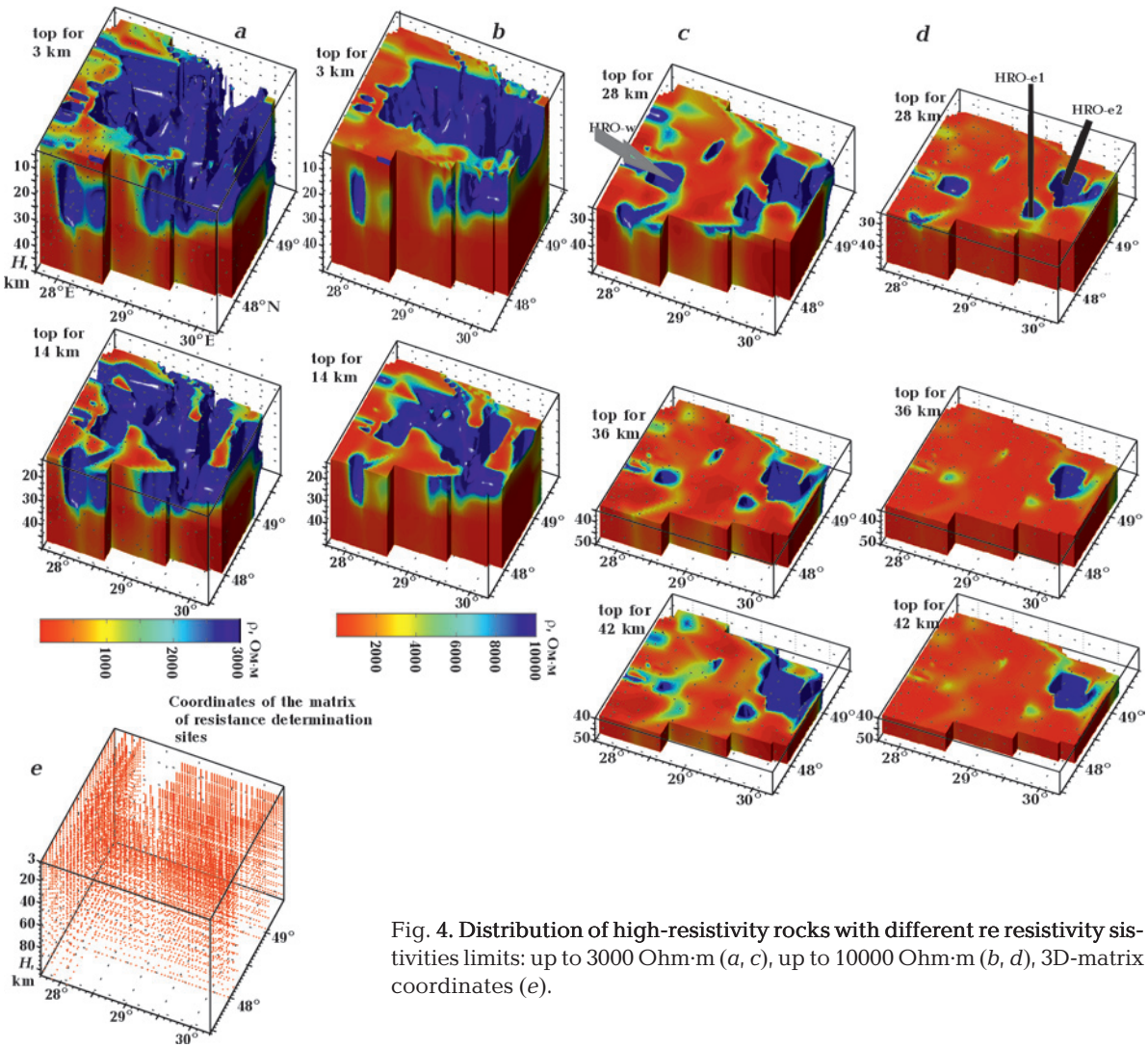

Fig. 4. Distribution of high-resistivity rocks with different re resistivity sistivities limits: up to 3000 Ohm·m (*a*, *c*), up to 10000 Ohm·m (*b*, *d*), 3D-matrix coordinates (*e*).

appear as local objects (see Fig. 4, *d*). Two local high-resistivity objects remain in the mantle deeper than 50 km, practically disappearing at a depth of 100 km (see Fig. 4, *e*).

In the western region (to the west of 28.5° E) in the depth interval of 15—30 km, a high-resistance block (HRO-w) with a resistivity of more than 4000 Ohm·m is distinguished with a center at 28.2° E and 48.2° N (see Fig. 4, *b*, *d*). The horizontal dimensions of HRO-w decrease by several times with increasing depth from 28 to 50 km. In the central part, the resistance is more than 10000 Ohm·m, and their area decreases several times in the same depth interval. In the eastern region (east of 29° E), there are two HROs with a resistance of over 3000 Ohm·m centered at 29.4° E/48.1° N (HRO-e1) and 29.7° E/48.7° N (HRO-e2). The central part of both blocks is a cylindrical body with a resistance of more than 10000 Ohm·m; its horizontal dimensions practically do not change in the depth interval of 28—50 km.

Against the background of high-resistivity rocks, low-resistivity objects stand out. In practice, the SURFER program is usually used to visualize area data. Rock resistivity in the studied volume varies in a very wide range from units to tens of thousands Ohm·m, which greatly complicates interpolation in the SURFER program. To facilitate the construction of the distribution ρ on slices, one can reduce the bit depth of the change in resistance using the values of Lgρ.

Even the Roman poet Horace wrote «Est modus in rebus», which in a free translation means «There is a measure in things, there are, finally, boundaries on either side of which there can be no truth». Therefore, before building a volumetric geoelectric model, considering the above points, a comparison was made of the distribution of LRO at different depth slices obtained using the SURFER program and using manual interpolation to identify LRO (Fig. 5).

With the manual method, the allocation of LRO was carried out at points where was less than 120 Ohm·m. The LRO contours are drawn taking into account the Kotelnikov-Nyquist-Shannon theorem (which applies to both time

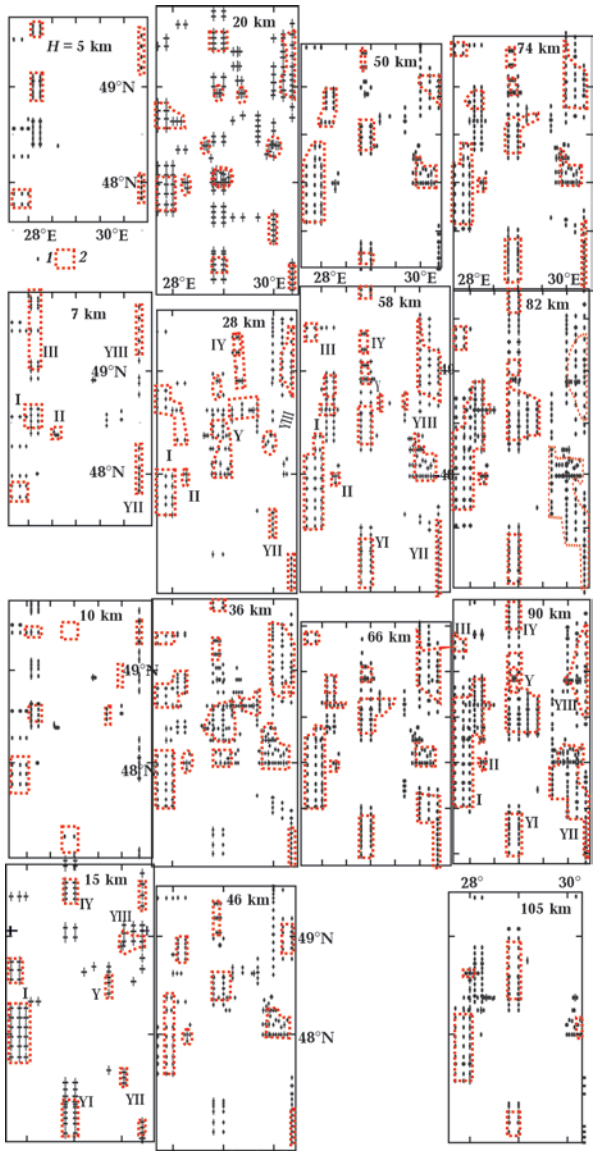

Fig. 5. Distribution of LRO on slice maps: *1* — points with values ρ<200 Ohm·m, *2* — contour of areas with resistivities values in points less than 100 Ohm·m. Roman numerals — LRO numbering.

and space functions). According to the theorem, having at least three discrete samples is preferable to select an object. When drawing the 100 Ohm·m isoline, the distances between the points were considered, comparable in size to the inversion cells and the distance between the interpretation profiles.

The pattern underlying the distribution of LRO in space and depth can best be traced on slice maps in the depth interval from 5 to 105 km. First of all, to determine the presence of the number of points with values

of ρ<120 Ohm·m and their distribution in space, a manual drawing of 100 Ohm·m isoclines (contour LRO) on slice maps (Fig. 6) was performed. For the correct drawing of the 100 Ohm·m isoline, interpolation was carried out for all points of this slice with ρ<200 Ohm·m. Slicing maps show LROs characterized in the horizontal plane by at least 3 points and traced in consistent coordinates at least at two adjacent depths. LROs in which points with values of ρ<120 Ohm·m are located only along one line, but stand out on several successive slices, are called alleged objects (LROa).

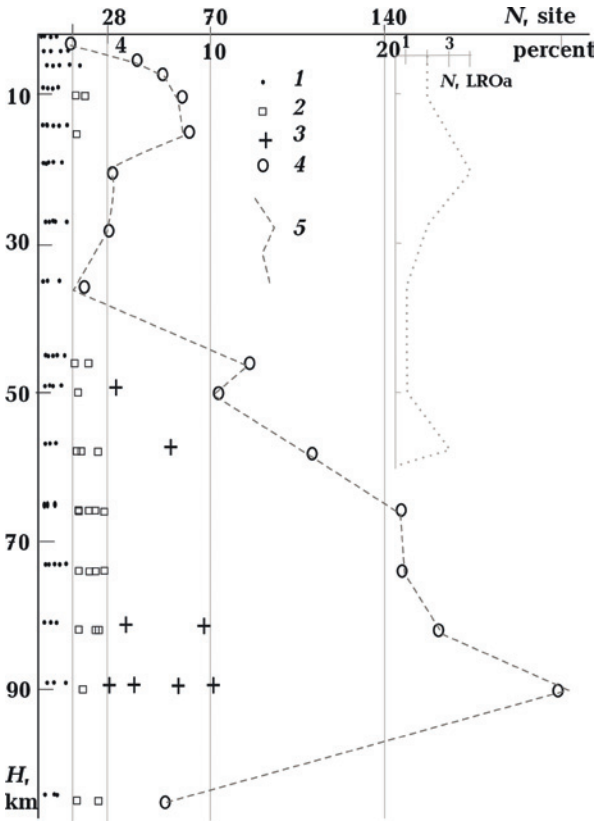

Fig. 6. The number of points of determination ρ, along which the isoline ρ=100 Ohm·m was drawn (*a*): *1* — 3—14, *2* — 15—28, *3* — 29—70, *4* — all, *5* — as a percentage of the total number of points on the cut. The number of LROa objects (*b*).

Thanks to data on geoelectric parameters at great depths, it is possible to reveal the genetic relationship of LROs isolated at the depths of the Earth's crust with sources in the upper mantle. In the interval of 60—90 km, 7 LROs are distinguished, characterized by the largest areas and quite close in position in space. At depths of 46—58 km, LRO-I disappears, and the areas of the remaining LROs decrease. At depths less than 40 km, LRO-YI and YII are either completely absent or appear as LROa (at depths of 5—15 km), while LRO-II breaks up into several small-sized objects. Data from MT studies at latitudes south of 47.5° N small, so LRO-Y is correctly identified only at depths greater than 54 km. LRO-III and IY are completely absent at depths less than 10 km and occasionally stand out at depths of 10—40 km. At depths of 5—15 km, LRO-I appears, and its area is maximum in the depth interval of 6—11 km. The absence of MT data in the interval 28.3—28.70° E does not allow for estimating the degree of connectivity of LRO-I and LRO-III, as well as LRO-II and LRO-IY.

An estimate of the distribution of the number of points for which LROs were identified using manual interpolation is shown in Fig. 6 (the number of points, N, and their percentage with all points on the slice are plotted along the abscissa). A sharp increase in the points at which LROs are identified is observed in the depth interval of 45—60 km (i.e., in the zone of transition from the crust to the mantle). The maximum number of points (more than 20 %) forming the LROs is observed in the depth interval of 65—90 km. At depths exceeding 100 km, the number of LROs and their generating points decrease almost five-fold compared to the overlying depths of the upper mantle. It is interesting to note (see Fig. 6, *b*) that at depths of 5—28 km, a significant amount of LRO is released, while such objects are absent at depths of the upper mantle. The allocation of LRO at these depths is due to the fact that their position coincides with LRO at greater depths.

The above signs indicate that there are local conductive objects at the depths of the Earth's crust and that no objects can be attributed to the conductive layer. The highest density of small-sized LROs is observed in the depth interval of 25—40 km in the area between 48—49.4° N and 28.8—29.8° E. In the interval of 58—90 km, the situation changes significantly — the number of points forming

LROs increases, and the areas occupied by LROs increase, but even here LROs do not form a connected layer. So the central part of one of the largest LRO-I in the depth interval of 50—100 km stretches for 88 km along the meridian with a width of about 30 km. The nearest LRO-III, Y, and YI are located at distances of about 30 km.

Given the small (compared to the total number of points) number of points for which LROs were allocated, a procedure was carried out for comparing the construction of slice maps using the Kriging interpolation method of the SURFER program (which is used in many works) and manual interpolation (Fig. 7). The comparison was made for depths with a different number of points (28 at a depth of 28 km, 65 at a depth of 28 km, 80 at a depth of 46 km, 150 at a depth of 66 km, and 170 at a depth of 82 km), for which LROs were identified.

The Kriging method builds a statistical model of reality rather than an interpolation function model [Maltsev, Mukharamova, 2014]. The method is an exact interpolator (if no smoothing parameter is specified).

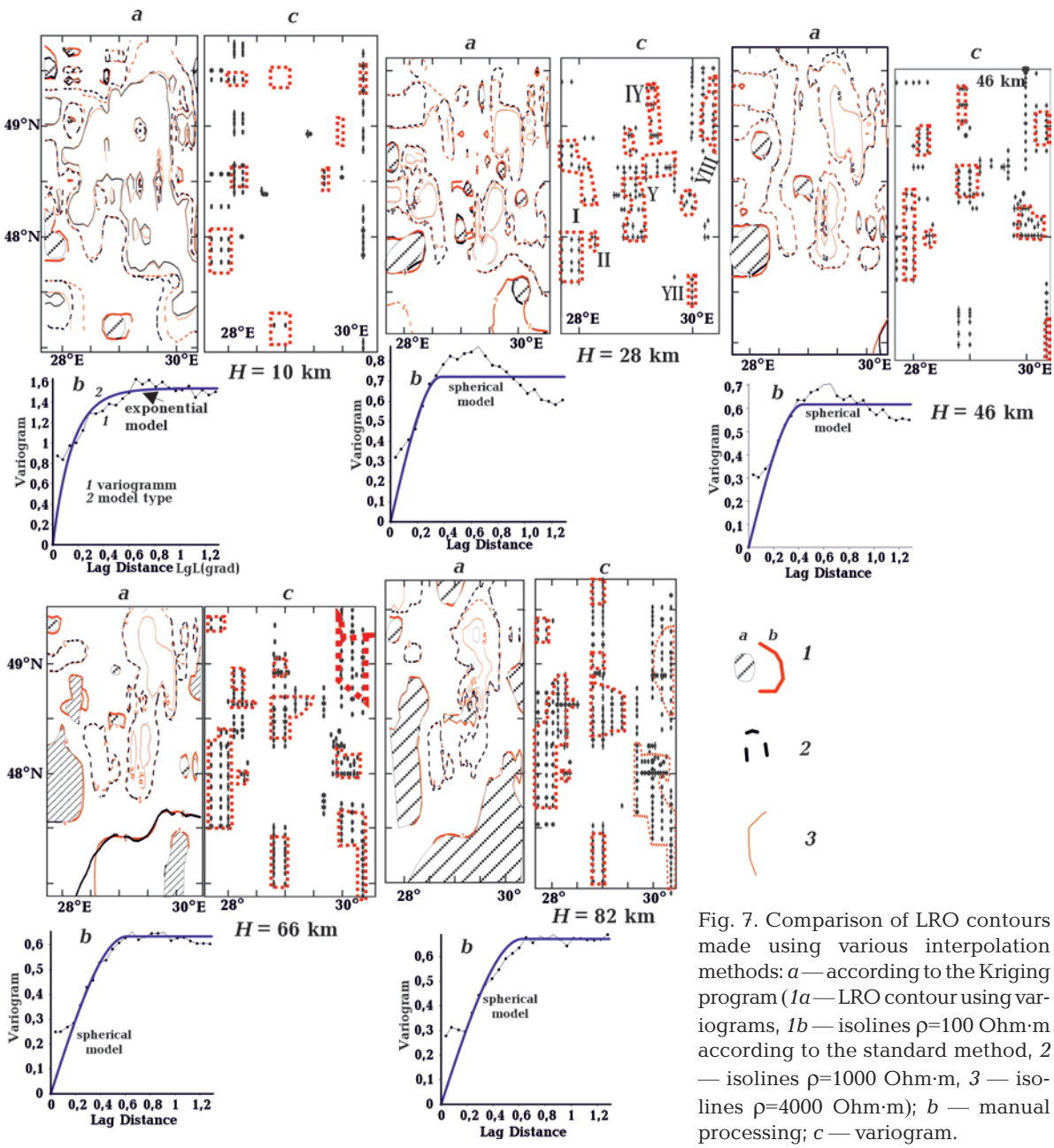

Fig. 7. Comparison of LRO contours made using various interpolation methods: *a* — according to the Kriging program (*1a* — LRO contour using variograms, *1b* — isolines ρ=100 Ohm·m according to the standard method, *2* — isolines ρ=1000 Ohm·m, *3* — isolines ρ=4000 Ohm·m); *b* — manual processing; *c* — variogram.

Fig. 7, *a* shows the fit results for the used data matrix (see Fig. 4) using the Kriging program on the standard model and using semivariograms. Fig. 7, *c* shows the best semivariogram models: exponential for depths of 10 km and spherical for other depths. All Fig. 7, *b* show LRO models for depths for which models were built using the Kriging program.

On the 10 km section, the centers of the LROs identified by both methods more or less agree, but their areas vary greatly (except LRO-I, YI, and YIII). Kriging according to the standard method gives a larger LRO than Kriging using semivariograms. On the cut of 28 km, the positions of the LRO centers are close, but only for LRO-I and YII are the areas

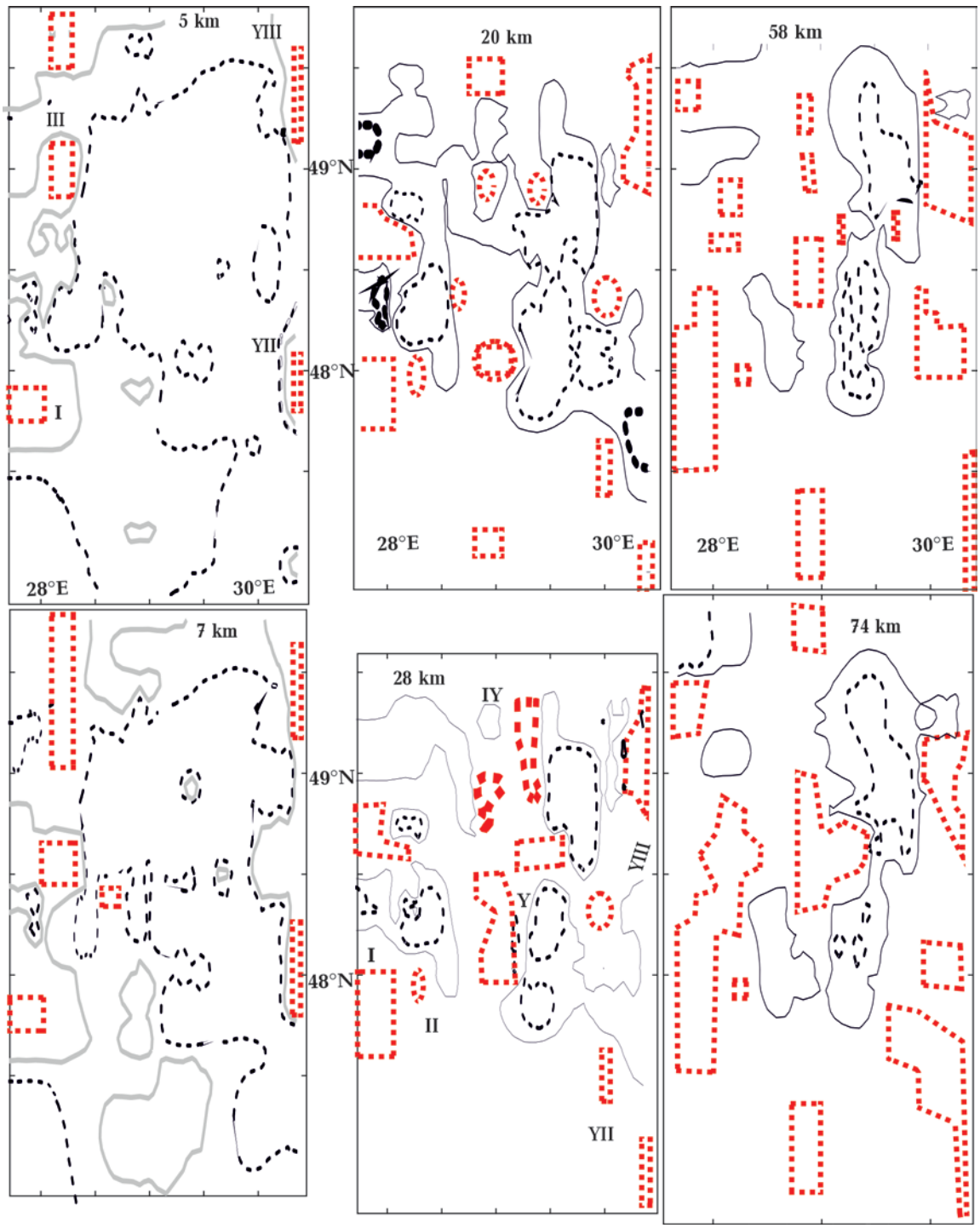

consistent. Contours isolines ρ=100 Ohm·m made using various interpolation methods to the Kriging program are almost the same. On the 46 km section, the positions and areas of LRO-I, Y, and YII and YIII are almost consistent and differ strongly for LRO-I, IY, and YI. Contours isoclines ρ=100 Ohm·m made using various interpolation methods to the Kriging program are almost the same. On the 66 km section, the centers of the LRO objects are more or less consistent, but the areas are close only for LRO-I and YII. Contour isolines for ρ=100 Ohm·m made using various interpolation methods to the Kriging program are almost the same. On the 82 km section, the centers of the LRO objects are more or less

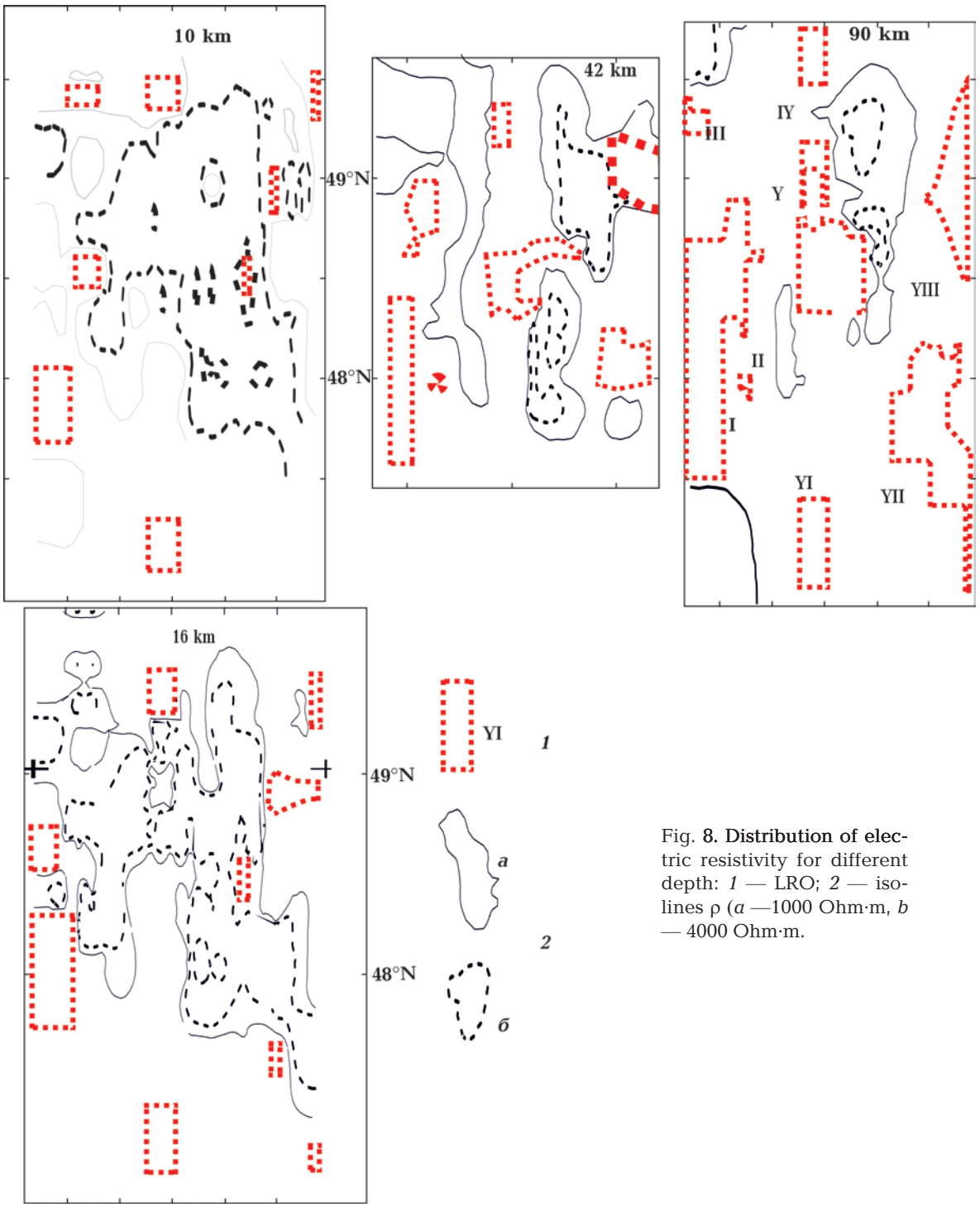

Fig. 8. Distribution of electric resistivity for different depth: *1* — LRO; *2* — isolines ρ (*a* —1000 Ohm·m, *b* — 4000 Ohm·m.

consistent. Areas LRO-I are consistent, LRO-YI, YII, in principle, consistent with the object selected by the SURFER program, but the interpolation in the latter was not performed correctly.

Using both methods to construct resistivity maps showed that with an uneven network of observations and the number of points with resistivity less than 100 Ohm·m (much lower than at most other points), LRO boundaries are poorly distinguished during interpolation in SURFER. Where LRO objects identified in different ways are close, better agreement of LRO boundaries is observed according to the Kriging program using interpolation method variograms. Contours of resistance isoclines over 1000 Ohm·m using various interpolation methods to the Kriging program almost coincide.

The distribution patterns of LRO and HRO in space are well traced on slice maps in the depth interval of 3—105 km (Fig. 8). Considering the process of the appearance of LROs, one can see a decrease in their parameters with approaching the Earth's surface and a decrease in the parameters of high-rise objects with depth.

In the interval of 60—90 km, seven LROs are distinguished, characterized by the largest areas and quite close in space. At depths of 46—58 km, LRO-I disappears, and the areas of other LROs decrease. At depths less than 40 km, LRO-YI, YII are almost completely absent, and LRO-II breaks up into several small objects. Data from MT studies at latitudes south of 47.5° N few, so LRO-Y is correctly identified only at depths greater than 54 km. LRO-III and IY at depths less than 10 km are completely absent and occasionally stand out at depths of 10—40 km. At depths of 5—15 km, LRO-I appears, with its area largest in the depth range of 6—11 km. No MT data are available for the interval 28.3—28.70W. This does not allow assessing the degree of connectivity of LRO-I and LRO-III, as well as LRO-II and LRO-IY.

It should be noted that there is a clear genetic link between LRO and HRO. The appearance of low-resistivity objects of considerable area and thickness in the mantle testifies to modern activation. The decrease in the size of the LRO as it approaches the Earth's surface may be due to the upward penetration of low-resistance inclusions associated with the mantle source.

The position of the LRO is controlled by high-resistivity (ρ>4000 Ohm·m) columnar objects, the resistance of which corresponds to near-surface crystalline rocks. So around the central part of HRO-w up to 30 km, several small LROs formed from LRO-I. Below 30 km, HRO-w disappears as the LRO-I area increases. A similar situation is observed in the eastern region. In the lower part of the Earth's crust, where the boundaries of HRO-e1 and HRO-e2 are clearly visible, the relationship between LRO and the latter is also clearly visible. The difference from the western region lies in the fact that despite the increase in the size of LRO-Y, YI, YII, and YIII, the objects HRO-e1 and e2 are preserved throughout the entire depth studied, only decreasing in size. It is most likely that crystalline high-resistivity rocks are characteristic of the most ancient deposits.

Thus, the spatial dimensions of the LRO zones indicate their locality and do not correspond to the layer's definition. In this case, it is very difficult to estimate the conductivity of local objects. If we apply the formula for the layer and take the average value ρ=40 Ohm·m, then the values of S can be approximately estimated at a thickness of about 50 km for LRO-I, Y, YII, and YIII equal to 1200 S, and for the rest of LRO it is much less.

Discussion and conclusions. When explaining the nature of conduction anomalies, it is useful to recall the saying of ancient philosophers: «De nihilo nihil». Marcus Aurelius interpreted this expression more broadly: «Nothing comes out of nothing, just as nothing passes into nothing». Below is an analysis of the reasons for the resistance values of various rock types.

In [Gordienko, 2001], a classification of the reasons for the appearance of conducting objects is proposed. The most common classification is carried out according to the types of low-resistivity inclusions in the volume of high-resistivity rocks (crystalline

basement): «…. crystalline rocks with a melt with practically no fluid or a significant role of fluid, ancient rocks with inclusions of graphite and ore, relatively young (and less metamorphosed) rocks with semi-anthracite, anthracite, shungite, and graphite and ore». In addition to this approach, V.V. Gordienko proposes to make the classification historical-genetic, i.e., «to distinguish conductors associated with 1) ancient processes, the active thermal phase of which has long passed and modern T is below solidus temperatures and dehydration of rocks; 2) modern active processes corresponding to deep heat and mass transfer and accompanying phenomena; 3) for a long time (over many cycles of activation) by existing zones of release or storage of thermal energy, where temperatures exceed the solidus of rocks».

The obtained three-dimensional geoelectric model can be compared with geological ideas about the composition of the crystalline rocks of the USh crust. In the region, rocks of various metamorphism facies are exposed (or are under sedimentary deposits less than 250 m thick, Fig. 1): Archean, Early, and Late Proterozoic [National…, 2007] (Fig. 9, *a*). These rocks were formed at temperatures and pressures corresponding to depths of 7—37 km. In [Gordienko et al., 2005], «the distribution of temperatures (T) in the crust of the USh by depth (pressure) was constructed, which corresponds to the conditions of regional metamorphism. Then, according to the typical values of T for each facies and subfacies, the characteristic depth interval (ΔH) was determined for them. The average depth value in the interval is assigned to the area of distribution of the facies or subfacies». Fig. 9, *b* shows «a map of the depths of the ero-

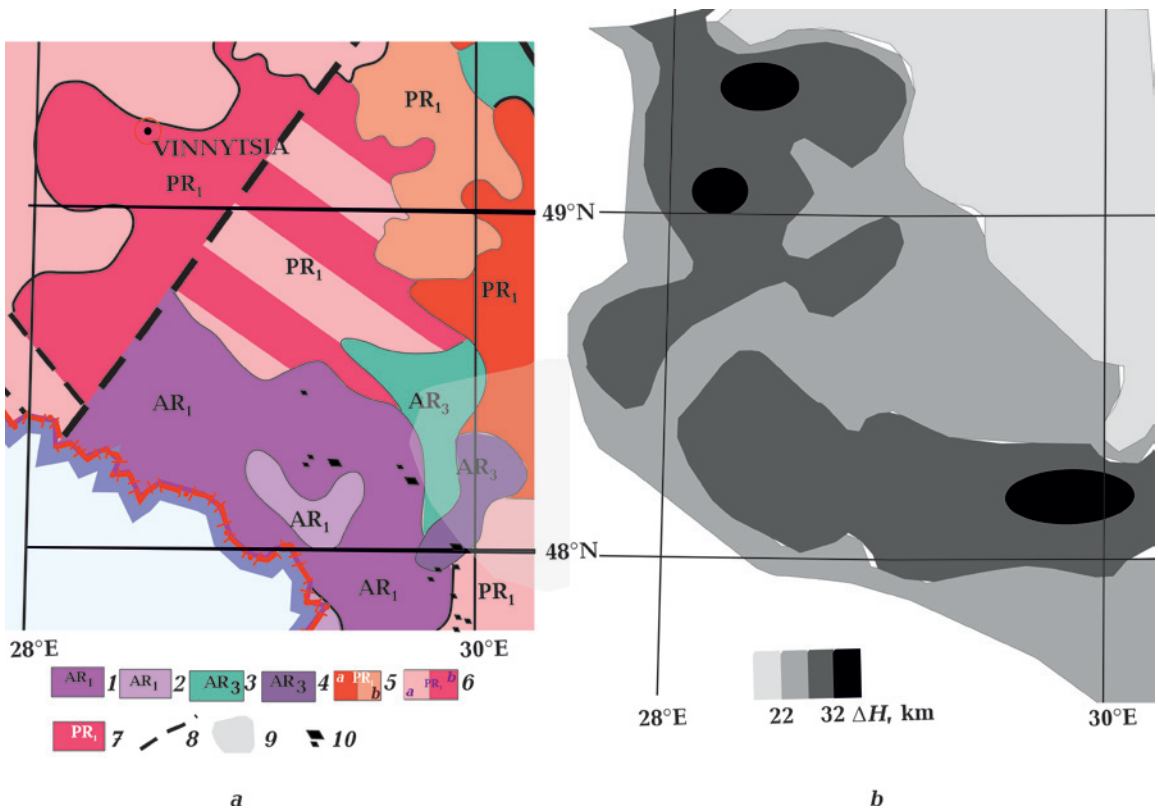

Fig. 9. Geological map of pre-Riphean deposits [National…, 2007] (*a*): *1* — enderbites; *2* — gneisses, crystalline schists, amphibolites, calciphyres, ferruginous quartzites, mafic rocks, ultramafic rocks; *3* — plagiogranites, diorites, granodiarites, gneisses, amphibolites; *4* — gneisses, ferruginous quartzites, marbles, crystalline schists, gabbro, peridotite, pyroxenites; *5* — granites (*a*), migmatites (*b*); *6* — granites, migmatites (*a*), charnockites (*b*); *7* — granites, migmatites, granodiorites, diorites; *8* — regional faults; *9* — Srednebugsky graphite-bearing area [Yatsenko, 1998]; *10* — manifestations of graphite content [Taranyuk, 1981]. The depths of the erosion cut of the Ukrainian Shield according to V.V. Gordienko [Gordienko et al., 2005] (*b*).

sion cut of the shield, the isoclines on which are drawn every 5 km, which corresponds to a threefold error in determining ΔH».

The outcropping Precambrian rocks of the Dniester-Bug megablock belong to the Pobug structural-facies complex (SFC) of the charnockite-granulite type (see Fig. 9, *a*). The further description is taken from the Explanatory Note to [Gurskiy, Kruglov, 2007]. In the vertical section of the SFC, four main breed associations are identified. The lower one is gneiss-kintzigite, about 2 km thick. Overlying are rocks of the gneiss-enderbite association, about 3 km thick, consisting of hypersthene gneiss-crystal schist and gneiss-enderbite formations. The third association includes gneiss-leucogranite, 3—4 km thick, consisting of laterally conjugated supercrystal leucogranulite and ultra metamorphic gneiss-alaskite formations. The SFC section ends with a thick layer of formations consisting (from bottom to top) of the following formations: high-alumina-quartzite (quartzite, silimanite, often with graphite, gneiss, and crystalline schist), 0.8—1.2 km thick; marble-calciphyre, 0.7—1.5 km thick; kondalitic (graphite-bearing, graphite and biotite-graphite gneisses, magnetite-hypersthene-garnet-quartz rocks) with a thickness of 0.3—0.4 km; eulysite (garnet and hypersthene gneisses, plagiogneisses, two-pyroxene, and hornblende-two-pyroxene crystalline schists), about 2.5 km thick.

Thus, the total thickness of the SFC rocks is about 14 km. Little is known about the lithology of rocks in the deeper horizons of the Earth's crust. In the monograph by Shcherbakov [Shcherbakov, 2005] based on xenoliths in gabbro at depths greater than 15 km, the presence of metamorphosed rocks from granulite to eclogite is assumed. The least metamorphosed contain half of the plagioclases, the rest — pyroxenes and garnets, and the most metamorphosed — only clinopyroxenes and garnets.

Fig. 10 shows the results of laboratory studies of the dependence of 1/ρ values on temperature for rocks of the Earth's crust. In [Shepel, 2003], measurements were made for rock samples from the region of the present study. The review by Yang [Yang, 2011] presents laboratory data on the dependence of 1/ρ values on temperature for the main minerals of rocks «depth of the lower continental crust is 15—25 to 40 km (the Moho discontinuity)», which are supplemented by data from [Dai et al., 2020]. The data show that the resistivity of the above types of rocks for the study region in the upper horizons of the Earth's crust at temperatures below 300 °C is much more than 10^5 Ohm·m. In the lower horizons of the Earth's crust, where temperatures approach 400 °C, the resistivity of pyroxenites and gabbro remains above 10^5 Ohm·m, while for other rocks, itapproaches 10^4 Ohm·m.

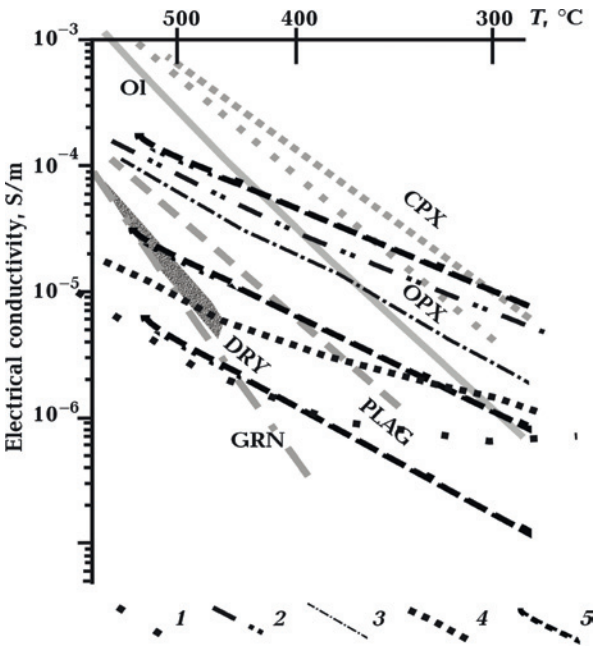

Fig. 10. The dependence of the conductivities of rocks and minerals in the lower part of the Earth's crust on temperature (*T*). Data are from [Shepel, 2003]: *1* — eclogite, *2* — basalt, *3* — migmatite, *4* — pyroxenite, *5* — gabbro; from [Yang, 2011]: CPX — clino-pyroxene, OPX — ortho-pyroxene, PLAG — plagioclase, dotted line with the same H_2O content and dry (DRY); from [Dai et al., 2020]: GRN — garnet, Ol — olivine.

Increased content of minerals with an electronic type of conductivity, fluids in the Earth's crust and upper mantle, partial melting, and diffusion of volatiles can cause low values of ρ at various depths. As a result of laboratory studies, it has been shown that aqueous fluids can have ρ values in the range of 0.01—

10 Ohm, depending on the temperature and pressure gradient [Unsworth, Rondenay, 2012; Manning, 2018, etc.]. Melt ρ values depend on the amount of dissolved water and petrology and are usually estimated in the range of 1—0.1 Ohm [Unsworth, Rondenay, 2012; Laumonier et al., 2017, etc.]. The resistivity of rocks containing these inclusions does not exceed 120 Ohm·m.

The distribution of geoelectric parameters at depths up to 15 km agrees with the data presented. It is natural to assume that the discovered deposits of highly conductive minerals in the near-surface rocks of the territory, such as graphite-bearing rocks (see Fig. 9, *a*), are associated with ancient processes. The size and depth of the deposits (see Fig. 9, *a*) do not allow to detect their relationship with the constructed geoelectric model at the existing scale and depth (the initial depth of the model is at least 3 km) of MT studies.

Based on the obtained distribution of high-resistivity objects, it can be assumed that they are related to the rock composition. To do this, we will use the results of laboratory studies presented on the summary graph of the dependence of conductivity on the mineral composition of rocks (see Fig. 10, *a*). According to the graph, at temperatures assumed in the Earth's crust of the region, less than 500 °C [Gordienko, 2017], the values of resistances over 10^4 Ohm·m should correspond to rocks dominated by pyroxene and garnet. These minerals have an increased density (more than 3.3 g/cm^3), which should be reflected in the magnitude of the gravitational field.

In Fig. 11, a comparison of data on the gravitational field of the territory with the distribution of the highest conductivity objects (more than 4000 Ohm·m) at the depths of the Earth's crust is given. The above comparison shows that tall objects are consistent with positive Bouguer anomalies. The HRO-w object is more or less consistent with the Bouguer anomaly greater than 30 mGal in the depth interval of 16—30 km. The HRO-e1 object is consistent with a Bouguer anomaly greater than 30 mGal in the depth interval of 10—42 km, and the HRO-e2 object is consistent with a Bouguer anomaly greater than 20 mGal in the depth interval of 10—90 km (see Fig. 8).

Against the background of high-resistivity rocks, objects of reduced resistance are distinguished in the entire investigated thickness, the distribution of which by area and depth is shown in Fig. 4, 8. The spatial distribution of LROs suggests a genetic relationship between mantle LROs and crustal ones.

Over the past 25 years, IGF has been studying zones of recent activation (ZRA) on the territory of Ukraine using a comprehensive interpretation of geological and geophysical data [Gordienko et al., 2005, 2020; Gordienko, 2017, etc.] and a variant of the distribution

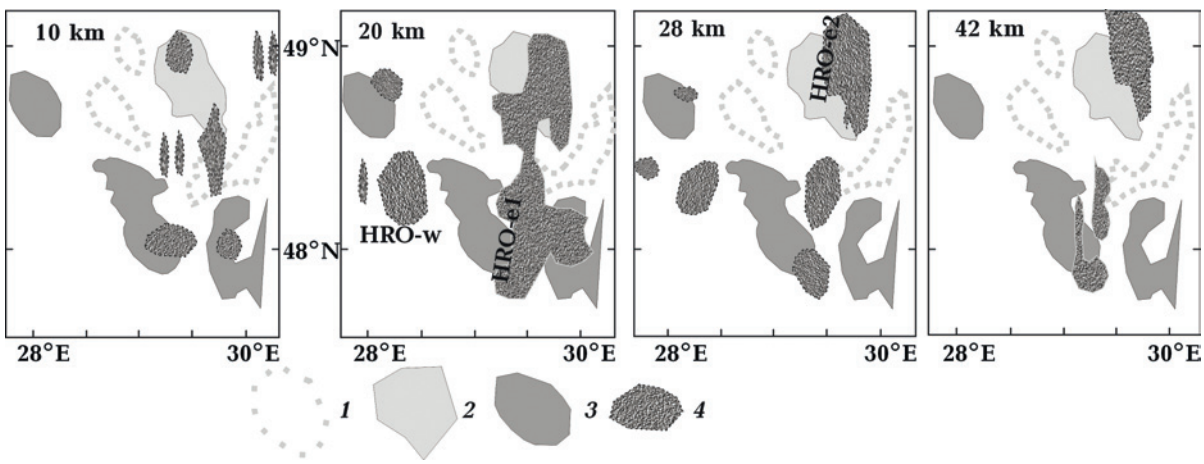

Fig. 11. Comparison of Bouguer anomaly values [National..., 2007]: *1* — 10 mGal, *2* — more than 20 mGal, *3* — more than 30 mGal, *4* — with rock distribution with rvalues of more than 4000 Ohm·m. HRO — high blocks stretching to great depths (see Fig. 4).

of ZRA on the territory of Ukraine has been constructed to date, including 12 zones [Gordienko et al., 2020]. One of these zones (Beltska ZRA) was identified in the southern part of the studied region.

Fig. 12 compares Beltska ZRA with the distribution of resistances at a depth of 74 km. The cut depth corresponds to the depth of the central part of the zone of partial melting of the corresponding thermal model. The lack of a complete set of geological and geophysical data on the territory of Moldova did not allow determining the boundaries of the ZRA outside the territory of Ukraine. However, the available definitions of the heat flow (see Fig. 12) show that the zone also extends to the territory of Moldova. From the above comparison, it can be seen that LRO-I, II, Y, and YII clearly agree with the ZRA boundary, which is identified with a probability of 75—100 %, and LRO-YIII enters the zone identified with a probability of 50 %.

To explain the reduced resistivities of the identified LROs, overheating of the rocks to solidus and 2—3 % melting and/or the presence of fluids is necessary [Gordienko, 2017]. The works [Karato, 1990, 2006] showed that when hydrogen diffuses into olivine, the resistivity of rocks changes by almost an order of magnitude when the temperature changes from 1200 to 1400 °C (according to the thermal model, it is precisely this temperature range at depths of more than 60 km that is assumed in the Beltska ZRA [Gordienko, 2017]. In recent studies discussing the influence of thermobaric conditions and the content of fluids necessary to explain the presence of increased conductivity in the upper mantle, the authors [Blatter et al., 2022] concluded that an anomalously large amount of volatiles is needed with small amounts of melt. Such a composition of the melt in the mantle will be more mechanically stable.

In recent years, the world has paid much attention to studying deep hydrogen degassing of the Earth and searching for geological structures in which it can be detected. In works devoted to this issue, it is noted that the processes of areal degassing of the Earth are associated with areas of tectonic activation

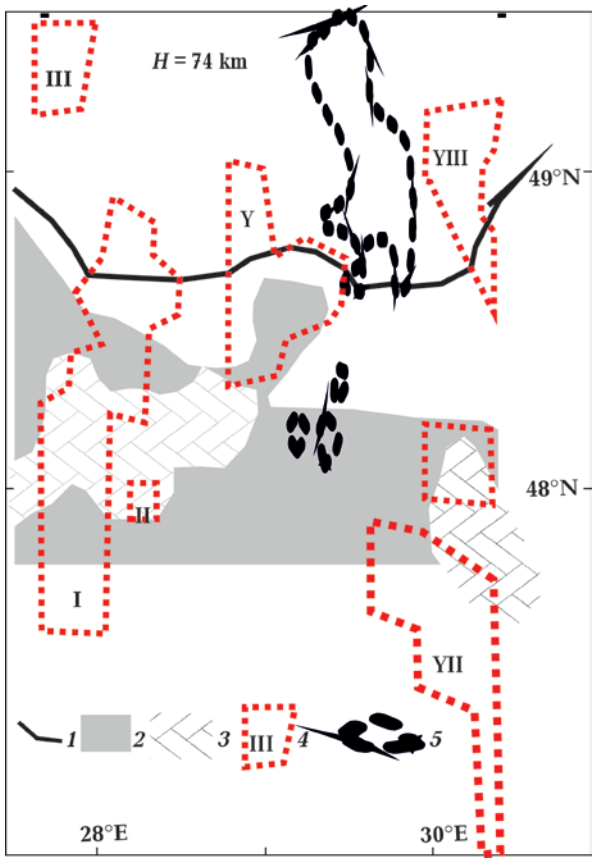

Fig. 12. The Beltska zone of recent activation, identified according to regional criteria (the boundaries of areas with a probability of activation of 50 % (*1*), 75—100 % (*2*), 100 % (*3*)) [Gordienko, 2017] and the distribution at a depth of 74 km of LRO (*4*) and HRO, ρ>4000 Ohm·m (*5*) objects.

[Shestopalov et al., 2018; Gordienko, 2021, etc.]. In rocks with low permeability (igneous, metamorphic) at a sufficient depth, the gas remains indefinitely without participating in the creation of a flow through the surface. In zones of active (including geologically long-term) faults, hydrogen flows of varying intensity are often recorded.

As the experience of our previous studies showed, objects LRO are most often concentrated along deep faults or their intersection. It is the faults, first of all, that act as the main ways of unloading fluid flows coming from the deep bowels of the Earth. Using different approaches, comparison of fault zones shown on various geological and geophysical maps confiRMS the conclusion made by leading Ukrainian geologists [Gurskiy, Kruglov, 2007] «Regarding ... lateral inhomogeneities of the

Earth's crust, fault systems can have an intra-block, inter-block, and trans-block character. Without a comparative analysis of the features of the geological structure of adjacent block structures, the recognition of fault systems of such categories is almost impossible. Therefore, the «slicing» of megablocks and blocks, for giving preference to one or other discontinuous systems, will have a subjective nature».

Therefore, the geoelectric model for the depths of the Earth's crust was compared with fault zones, for which the authors describe the method of their identification and give the linear dimensions of the zones. Lineament zones of recent activation (LZRA) were identified as a result of morphographic and morphometric analyzes and processing of aerospace images [Verkhovtsev et al., 2012], and deep interblock zones of rank I faults [Entin, 2005] were identified by geophysical features (Fig. 13). In both works (as well as on all geological maps in general) the depth extension of the zones is not given.

Comparisons show (see Fig. 13) that up to depths of about 20 km, the distribution of the area of high-resistivity objects in space is controlled by interblock fault zones of rank I (Podolsk-III, Nemirov-IY, and Dashev-YI), and objects HRO-e1 and HRO-e2 are in good agreement with the Zvizdal zone from upper horizons of the Earth's crust up to 42 km. In the lower part of the Earth's crust (deeper than 20 km), good agreement between the LRO is observed with the Khmelnytsk fault zone of rank I (I), consistent with the Shepetivka-Ochakiv (62) LZRA and with the Letychiv-Obodivka (II). The LRO chain is observed along the Kryzhopil-Porozhbin (31) LZRA, and the sizes of individual LROs decrease from the lower horizons of the crust to the top. In the upper part of the crust, at depths less than 20 km, there is no clear relationship between LRO and the rest of the fault zones.

The depth extension of the fault zones can be estimated from seismological sections along the Bucharest-Chornobyl (B-Ch) and YI geotraverses. As can be seen from Fig. 14, *a*, the B-Ch profile is located almost along the Nemirov fault zone of rank I and is intersected by three lineament zones. The YI profile is located practically along the Kamen-Kashirsko-Yalta lineament zone, and the edges of the Odesa-Vinnytsia Early Proterozoic zone are consistent with the Khmelnytsk and Letychiv-Obodivka fault zones of rank I and are intersected by the rest of the fault zones. Fig. 14, *b* compares the position of the LRO

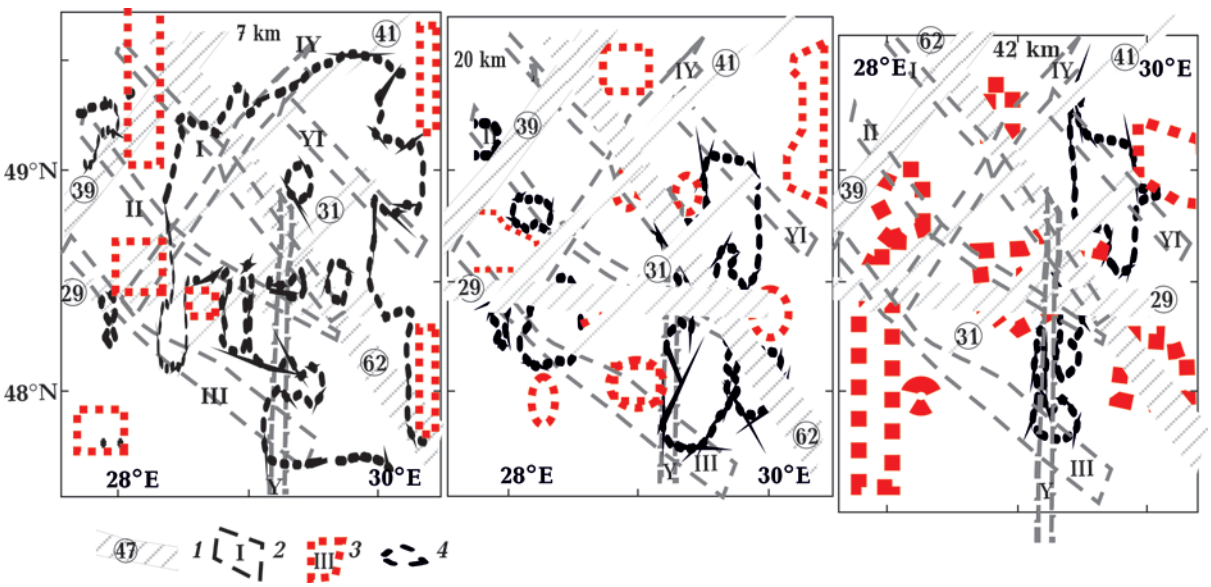

Fig. 13. Lineament zones of recent activation (zone numbers correspond to [Verkhovtsev et al., 2012]) (*1*), deep interblock fault zones of rank I according to [Entin, 2005] (*2*) (I — Khmelnytsk, II — Letychiv-Obodivka, III — Podolsk, IY — Nemirov, Y — Zvizdal) and resistance anomalies: LRO (*3*), isolines ρ=4000 Ohm·m (*4*).

zones at their intersections with seismic sections. Only the Mukachevo-Dnipro lineament zone is consistent with the fault zones identified from seismic data on both profiles. Taking into account the accuracy of the topographic reference of geological data, it can be argued that LRO-Y is in good agreement with this fault zone for almost the entire thickness of the crust. Both fault zones on profile YI southeast of PK400 agree with LRO-YII in position and depth. The agreement of LRO-III with the Muravan-Chornobyl lineament zone and fault zones is less reliable according to seismic data in the area of pickets 600 of the YI and B-Ch profiles (it should be taken into account that this territory is in the zone of absence of geoelectric data. The agreement is less reliable with the rest of the fault zones identified from seismic data.

Fig. 14, *c* «represents the results of the analysis of correlation dependences between the electrical and elastic properties of rocks under various thermobaric regimes on examples of studies of samples of migmatites, granites, gneisses, porferites and diabases» [Shepel, 2003]. Rock samples were taken from a 3,000 m deep well drilled in crystalline rocks in the central part of the Ukrainian shield. Comparison of the distribution of resistivity values with seismic sections shows good agreement between laboratory (see Fig. 14, *c*) and model geoelectric (see Fig. 8) data and seismic ones (see Fig. 14, *b*). Indeed, up to depths of less than 20 km (limited by the ve-

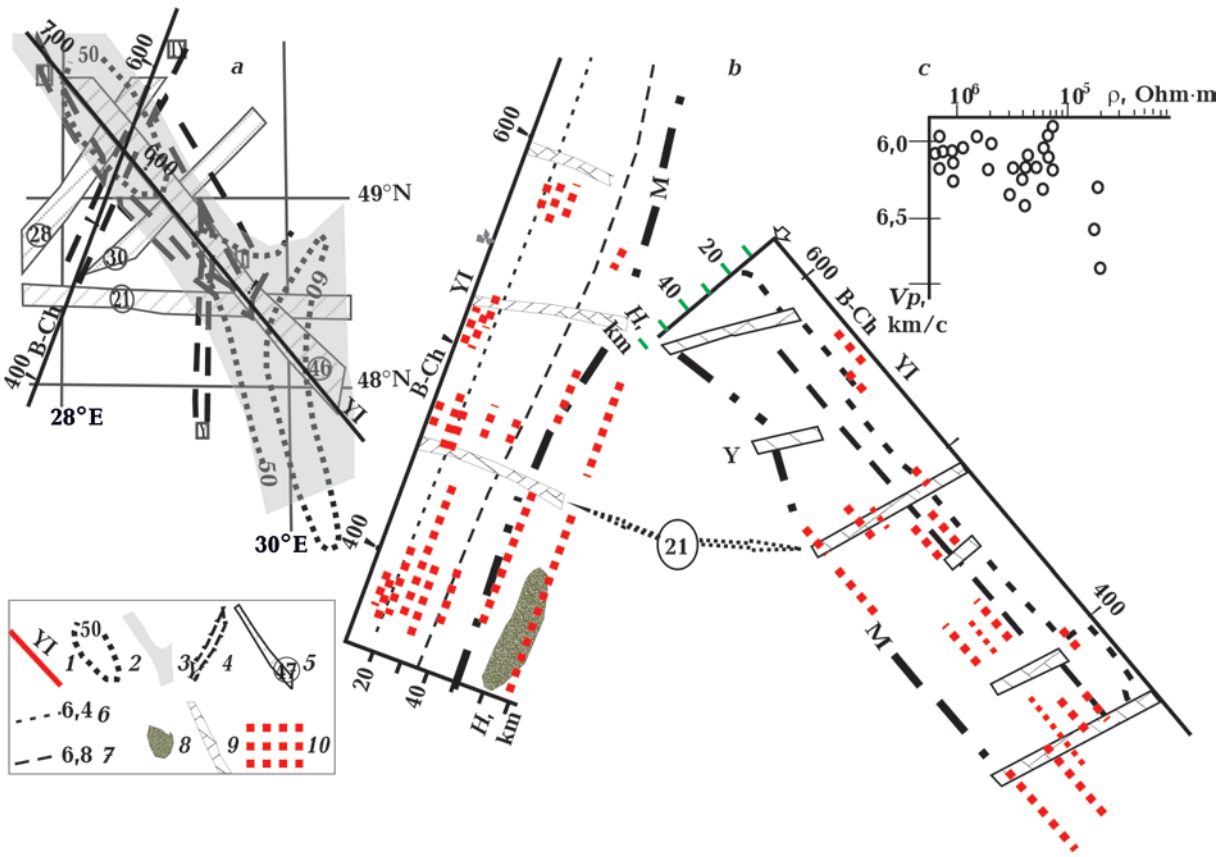

Fig. 14. Overview map of seismic data and fault tectonics (*a*): *1* — seismic profile lines; *2* — depth (km) of the Moho boundary; *3* — Odesa-Vynnitsia Early Proterozoic zone [Sollogub, 1986]; *4* — deep interblock fault zones of rank I according to [Entin, 2005] (I — Khmelnytsk, II — Letychiv-Obodivka, IY — Nemirov, Y — Zvizdal); *5* — lineament zones active in the Late Pleistocene-Quaternary time [Verkhovtsev et al., 2012] (numbers in circles): 21 — Mukachevo-Dnipro, 28 — Muravansko-Chornobyl, 30 — Mogilev-Podolsk-Shostka, 46 — Kamen-Kashirsko-Yalta. Seismic sections along the profiles Bucharest-Chornobyl (B-Ch) [Kharitonov et al., 1995] and YI [Sollogub et al., 1988] (*b*): *6*, *7* — velocities V_P (*6* — 6.4 km/s, *7* — 6.8 km/s); *8* — low velocity zone (V_P=7.8 km/s) in the mantle; *9* — fault zones according to seismic data; *10* — sizes of LRO. Relationship between electrical and elastic properties of rocks according to laboratory data [Shepel, 2003] (*c*).

locity isocline 6.4 km/s), rocks with a value of ρ over 4000 Ohm·m (HRO) are widespread throughout the entire territory, and deeper, their areas sharply decrease.

Conclusions. Using the experimental data obtained in recent years, we have built a new geoelectric model that characterizes the structure of the Earth's crust and upper mantle up to 100 km of most of the Dniester-Bug and adjacent megablocks of the Ukrainian shield. The presented model was obtained based on the results of a two-dimensional inversion (on six meridional and five latitudinal profiles) of the MT field interpretation parameters (in the period range from 1—9 to 1600—6400 s) obtained from magnetotelluric and magnetovariational soundings in 124 sites. The results of this study can be summarized as follows.

The entire block of rocks 200×200 km down to a depth of 100 km is characterized by high resistivity, against which objects of reduced resistivity are identified.

The resulting distribution of high-resistivity rocks over the entire depth of the model agrees with the laboratory dependencies obtained for the rocks of the Ukrainian Shield and other data. Model data show a significant difference in resistivities in the upper 14—16 km (above 10^5 Ohm), lower crust (about 10^4 Ohm), and upper mantle (10^3 Ohm). Against a general decrease in resistance with depth in the Earth's crust, three regions were identified in which anomalously high (for a given depth) resistivity extends to the entire thickness of the crust. These high-resistivity objects are consistent with positive Bouguer anomalies.

Against the background of high-resistivity rocks, LRO stand out, the resistance of which does not exceed 120 Ohm·m. The spatial dimensions of the LRO zones indicate their locality and do not form a cohesive layer. In this case, it is very difficult to estimate the conductivities of local objects. If we apply the formula for determining the total longitudinal conductivity of the layer and take the average value ρ=40 Ohm·m, then the values of S can be approximately estimated at an object thickness of about 50 km for LRO-I, Y, YII, YIII equal to 1200 S, and for the rest of LROs, it is much less.

An analysis of the distribution of LROs in space and depth suggests a genetic relationship between mantle LROs and crustal LROs. Comparison of mantle LROs with the Beltska zone of modern activation on the territory of Ukraine, identified using the integrated interpretation of geological and geophysical data, shows their good agreement both vertically and horizontally. To explain the lower LRO resistivity in the upper mantle, overheating of the rocks to solidus and 2—3 % melting and/or the presence of fluids is necessary [Gordienko, 2017]. In recent studies discussing the influence of thermobaric conditions and the fluid content necessary to explain the presence of increased conductivity in the upper mantle, the authors [Blatter et al., 2022] concluded that an anomalously large amount of volatiles is needed with small amounts of melt. Such a composition of the melt in the mantle will be more mechanically stable. The assumption that mantle LROs are related to crustal LROs has been tested by comparing LROs with fault zones. The presence of LROs in the mantle, their vertical extent, and their connection with rejuvenated fault systems can serve as a basis for the deep migration of fluids enriched in volatiles.

The conducted studies have shown that the geoelectric results can be important for carrying out a complex geological and geophysical interpretation.

In the future, to improve the geoelectric model, it is necessary to conduct experimental MT studies in the southern part of the Dniester-Bug megablock and the band between 28° and 29° E.

Acknowledgments. This work was carried out as part of project 0117U000117 «Deep processes in the crust and upper mantle of Ukraine and formation of mineral deposits» funded by the National Academy of Sciences of Ukraine. We are very grateful to V.V. Gordienko for fruitful discussions. We thank S. Kovachikova for constructive comments that greatly improved the manuscript.

References

Blatter, D., Naif, S., Key, K., & Ray, A. (2022). A plume origin for hydrous melt at the lithosphere-asthenosphere boundary. *Nature, 604*, 491—494. https://doi.org/10.1038/s41586-022-044483-w.

Burakhovich, T.K., Gordienko, I.V., Kulik, S.N., Logvinov, I.M., & Tarasov, V.P. (1997). Magnetotelluric studies of zones of young activization of the tectonosphere in the northern part of the Moldavian plate. *Geofizicheskiy Zhurnal, 19*(5), 44—49 (in Russian).

Dai, L, Hu, H., Jiang, J., & Sun, W. (2020). An Overview of the Experimental Studies on the Electrical Conductivity of Major Minerals in the Upper Mantle and Transition Zone. *Materials, 13*, 408. https://doi.org/10.3390/ma13020408.

Entin, V.A. (2005). Geophysical basis of the tectonic map of Ukraine at a scale of 1:1 000 000. *Geofizicheskiy Zhurnal, 25*(1), 74—88 (in Ukrainian).

Gordienko, V.V. (2001). Nature of crustal and mantle conductors. *Geofizicheskiy Zhurnal, 23*(1), 29—39 (in Russian).

Gordienko, V.V., Gordienko, I.V., Zavgorodnyaya, O.V., Kovachikova, S., Logvinov, I.M., Tarasov, V.N. & Usenko, O.V. (2012) *Volyn-Podolyan plate (Geophysics, deepprocesses)*. Kiev: Naukova Dumka, 198 p. (in Russian).

Gordienko, V.V. (2021). On the circulation of hydrogen in the atmosphere and the Earth's crust. *Geofizicheskiy Zhurnal, 43*(5), 35—59. https://doi.org/10.24028/gzh.v43i5.244051 (in Russian).

Gordienko, V.V. (2017). *Thermal processes, geodynamics, deposits*. 283 p. Retrieved from https://docs.wixstatic.com/ugd/6d9890_c2445800a51b49adb03b8f949f3d6abb.pdf.

Gordienko, V.V., Gordienko, I.V., Gordienko, L. Ya., Zavgorodnyaya, O.V., Logvinov, I.M., & Tarasov, V.N. (2020). Zones of recent activation of Ukraine. *Geofizicheskiy Zhurnal, 42*(2), 29—52. https://doi.org/10.24028/gzh.0203-3100.v42i2.2020.201740 (in Russian).

Gordienko, V.V., Gordienko, I.V., Zavgorodnyaya, O.V., Kovachikova, S., Logvinov, I.M., Tarasov, V.N., & Usenko, O.V. (2005). *Ukrainian Shield (Geophysics, deepprocesses)*. Kiev: Korvin Press, 210 p. (in Russian).

Gurskiy, D.S., & Kruglov, S.S. (Eds.). (2007). *Tectonic map of Ukraine M 1:1 000 000*. Kiev: UkrDGRI (in Ukrainian).

Ilchenko, T.V. (2002). Results of SEISMIC surveys along the Eurobridge-97 transept. *Geofizicheskiy Zhurnal, 14*(3), 36—50 (in Russian).

Karato, S. (2006). Influence of Hydrogen-Related Defects on the electrical conductivity and plastic deformation of mantle minerals: A Critical Review. In S.D. Jacobsen, S. Van Der Lee (Eds.), *Earths Deep Water Cycle* (Vol. 168, pp. 113—129). https://doi.org/10.1029/168GM09.

Karato, S. (1990). The role of hydrogen in the electrical conductivity of the upper mantle. *Nature, 347*, 272—273. https://doi.org/10.1038/347272A0.

Kharitonov, O.M., Omelchenko, V.D., Drogitskaya, G.M., & Kutas, V.V. (1995). The lithospheric transaction Bucharest-Chernobyl. *Doklady NAN Ukraine*, (5), 84—87 (in Russian).

Kovachikova, S., Logvinov, I., & Tarasov, V. (2022). Area-wide 2D and quasi-3D geoelectric models of the Earth's crust and upper mantle as a possible evidence of recent tectonic activity in the western part of the Ukrainian Shield. *Geodynamics*, (1), 99—118. https://doi.org/10.23939/jgd2022.02.099.

Ladanivskiy, B.T. (2003). Algorithm for processing MTZ data. *Fifth geophysical readings named after V.V. Fedynsky February 27 — March 01, 2003. Abstracts of reports* (pp. 134—135) (in Russian).

Ladanivskiy, B., Logvinov, I., & Tarasov, V.(2019). Earth mantle conductivity beneath the Ukrainian territory. *Studia Geophysica et Geodaetica, 63*(2), 290—303. https://doi.org/10.1007/sl1200-018-00347-4.

Laumonier, M., Blundy, J., Gaillard, F., Muir, D., & Unsworth, M.J. (2017). Giant magmatic water reservoirs at mid-crustal depth inferred from electrical conductivity and the growth of the continental crust. *Earth and Planetary Science Letters, 457*, 173—180. http://dx.doi.org/10.1016/j.epsl.2016.10.023.

Logvinov, I.M. (2015). Deep Geoelectric Structure of the Central and Western Ukraine. *Acta Geophysica, 63*(5), 1216—1230. https://doi.org/10.1515/acgeo-2015-0049.

Logvinov, I.M., & Tarasov, V.N. (2019). Electrical conductivity of the crust and mantle of the East European platform in the western part of Ukraine from area-wide 2D models. *Geofizicheskiy Zhurnal, 41*(1), 44—75. https://doi.org/1024028/gzh0203-3100.v.41i1.2019.158863 (in Russian).

Maltsev, K.A., & Mukharamova, S.S. (2014). *Building models of spatial variables (with using the Surfer package)*. Kazan: Edition of the Kazan University, 103 p. (in Russian).

Manning, C. (2018). Fluids of the Lower Crust: Deep Is Different. *Annual Review of Earth and Planetary Sciences, 45*, 67—97. https://doi.org/10.1146/annurev-earth-060614-105224.

National Atlas of Ukraine. (2007). Kyiv: Cartography, 440 p. (in Ukrainian).

Orluk, M.I. (2000). Spatial and spatio-temporal magnetic models of different-ranked structures of the lithosphere of the continental type. *Geofizicheskiy Zhurnal, 22*(6), 148—165 (in Russian).

Ryka, V., & Maliszewska, A. (1989). *Petrographic Dictionary*. Moscow: Nedra, 590 p. (in Russian).

Scientific Report. The project «The geomagnetic field under the heliospheric forcing. Determination of the internalstructure of the Earth and evaluation of the geophysical hazard produced by solar eruptive phenomena». (2013). Program IDEI, Contract 93/5.10.2011, Stage I—III. Institute of Geodynamics Romanian Academy, 28 p. Retrieved from http://www.geodin.ro/IDEI2011/engl/index.html.

Shcherbak, M.P., & Bobrov, O.D. (Eds.). (2006). *Mineral deposits of Ukraine. V. I. Metalliferous mineral deposits*. Kyiv-Lviv: «Center of Europe» Publishing House, 739 p. (in Ukrainian).

Shcherbakov, I.B. (2005). *Petrology of the Ukrainian shield*. Lvov: ZUKS. 366 p.

Shepel, S.I. (2003). Electrical properties of rocks in thermobaric conditions of the lithosphere and geoelectric models. *Doctor's thesis*. Kiev, 411 p. (in Russian).

Shestopalov, V.M., Lukin, A.E., Zgonnik, V.A., Makarenko, A.N., Larin, N.V., & Boguslavskiy, A.S. (2005). *Essays on the degassing of the Earth*. Kyiv: Itek Service, 631 p. (in Russian).

Shilova, A.M., & Bilinskiy, A.I. (1983).On the conductivity of the sedimentary cover of Central Europe. *Geofizicheskiy Zhurnal, 5*(2), 90—93 (in Russian).

Shumlyanskiy, V.A. (2007). Tectonic conditions of the Cimmerian epoch of ore formation of the East European platform. In *Scientific works of the Institute of Fundamental Research* (pp. 50—68). Kiev: Logos (in Russian).

Siripunvaraporn, W., & Egbert, G. (2000). An efficient data-subspace inversion method for 2-D magnetotelluric data. *Geophysics, 65*(3), 791—803. https://doi.org/10.1190/1.1444778.

Sollogub, V.B. (Ed.). (1988). *Lithosphere of Central and Eastern Europe. Geotraverse IY, YI, YIII*. Kiev: Naukova Dumka, 172 s. (in Russian).

Sollogub, V.B. (1986). *Lithosphere of Ukraine*. Kiev: Naukova Dumka, 184 p. (in Russian).

Sollogub, V.B., Chekunov, A.V., Tripolskiy, A.A., & Babinets, V.A. (1978). Results of the study of the deep structure of the Ukrainian shield. In V.B. Sollogub, A. Guterkh, D. Prosen (Eds.), *The structure of the Earth's crust and upper mantle in Central and Eastern Europe* (pp. 136—147). Kiev: Naukova Dumka (in Russian).

Sollogub, V.B., Ilchenko, T.V., Borodulin, M.A., Sologub, N.V., Guterkh, A., Matezhek, R., Perkhuts, E., Yanik, T., & Grad, M. (1988). Seismic field. In V.B.Sollogub (Ed.), *Lithosphere of Central and Eastern Europe. Geotraverses IY, YI, YIII* (pp. 67—70). Kiev: Naukova Dumka (in Russian).

Stănică, M., Stănică, D., & Marine-Furnică, C. (1999). The placement of the Trans-European Saturne zone of the Romanian territory by electromagnetic arguments. *Earth, Planets and Space, 51*, 1073—1078. https://doi.org/10.1186/BF03351581.

Taranyuk, M.F. (Ed.). (1981). *Graphite-bearing map of the Ukrainian shield*. Kiev: Publ. of the Ministry of Geology of the Ukrainian SSR (in Russian).

Tarasov, V.N., Logvinov, I.M., & Litvinov, D.A. (2013). Comparative analysis of graphical representation of 3D models based on magnetotel-

luric sounding data. *Geoinformatika,* (3), 1—8 (in Russian).

Tregubenko, V.I., Finchuk, L.L., & Beloshapskaya, N.V. (1989). *Results of regional works by the MTS method of the north-western part of the Ukrainian SSR*. Kiev: UTGF, 130 p. (in Russian).

Unsworth, M.J., & Rondenay, S. (2012). Mapping the distribution of fluids in the crust and lithospheric mantle utilizing geophysical methods. In D.E. Harlov, H. Austrheim (Eds.), *Metasomatism and the Chemical Transformation of Rock, Lecture Notes in Earth System Sciences* (pp. 535—598). Berlin: Springer Verlag.

Varentsov, Iv.M. (2007). Joint robust inversion of MT and MV data. In *Electromagnetic sounding of the Earth's interior* (Vol. 40, pp. 189—222). Elsevier.

Verkhovtsev, V.G. (2008). The newest platform geostructures of Ukraine and the dynamics of their development. *Doctor's thesis*. Kyiv, 423 p. (in Ukrainian).

Verkhovtsev, V.G., Yuskiv, Yu.V., & Shvaiko, V.G. (2012). Active in the newest development stage of linear geostructures of Ukrainian Shield and its slopes. *Technogenic and ecological safety and civil protection,* (5), 49—59 (in Ukrainian)

Yang, X. (2011). Origin of High Electrical Conductivity in the Lower Continental Crust: A Review. *Surveys in Geophysics, 32*(6), 875—903. https://doi.org/10.1007/s10712-011-9145-z.

Yatsenko, V.G. (1998). Regularities of the spatial arrangement of graphite manifestations on the Ukrainian shield. In *Aspects of mineralogy in Ukraine* (pp. 254—270). Kiev: GNC ROS (in Russian).

Геоелектрична модель земної кори та верхів мантії Дністровсько-Бузького мегаблока Українського щита

***І.М. Логвінов*, І.В. Гордієнко, В.М. Тарасов, А.М. Логвінова, 2023**

Інститут геофізики ім. С.І. Субботіна НАН України, Київ, Україна

Мережа довгоперіодичних магнітотелуричних і магнітоваріаційних даних (124 пункти) у діапазоні періодів від 9—16 до 2500—6400 років дала можливість дослідити геоелектричну будову земної кори й верхньої мантії більшої частини Дністровсько-Бузького та прилеглих до нього мегаблоків Українського щита. На підставі розрізів питомих опорів по профілях (з 2D інверсією) створено тривимірну матрицю питомих опорів території, обмеженої координатами 27,7°—30.4° E та 47,7°—49,4° N, яка охоплювала просторові координати кожного вузла сітки на кожному профілі, потужність комірок моделі та значення опору в комірці. В результаті були виявлені геоелектрично аномальні структури на різних глибинах — від 3 до 100 км.

Увесь блок порід 200×200 км до глибини 100 км характеризується високим питомим опором, на фоні якого виділяються об'єкти зниженого питомого опору (ЗПО).

Отриманий розподіл високоомних порід по всій глибині моделі добре узгоджується з лабораторними залежностями, отриманими як для порід Українського щита, так і з іншими даними. За модельними даними отримано значну різницю питомих опорів у верхній частині кори — 14—16 км (понад 105 Ом), нижній її частині (приблизно 104 Ом) і верхній частині мантії (103 Ом). На фоні загального зниження опору з глибиною в земній корі виділено три області, в яких аномально високі (для певної глибини) опори поширюються на всю товщу кори. Ці високоомні об'єкти узгоджуються з позитивними аномаліями Буге.

На фоні високоомних порід виділено об'єкти ЗПО, опір яких не перевищує 120 Ом·м. Просторові розміри зон ЗПО вказують на їх локальність і не утворюють суцільного шару. Аналіз розподілу об'єктів ЗПО в просторі та на глибині свідчить про генетичний зв'язок між ЗПО мантії та ЗПО кори. Порівняння мантійних ЗПО із ЗПО Бельцької зони сучасної активізації на території України вказує на їх добрий

збіг як за глибиною, так і в просторі. Для існування нижчих значень питомого опору ЗПО у верхній мантії необхідний перегрів порід до солідусу та 2—3 % плавлення та/або наявність флюїдів. У нещодавніх дослідженнях стосовно впливу термобаричних умов і вмісту рідини, необхідного для пояснення наявності підвищеної провідності у верхній мантії, зроблено висновок, що необхідна аномально велика кількість летких речовин з малими кількостями розплаву. Припущення, що об'єкти ЗПО мантії пов'язані з об'єктами ЗПО кори, перевірено шляхом порівняння таких об'єктів із зонами розломів.

Наявність об'єктів ЗПО в мантії, їх вертикальна протяжність і зв'язок з омолодженими системами розломів можуть слугувати основою для глибинної міграції флюїдів, збагачених леткими речовинами.

Ключові слова: земна кора і верхня мантія, Український щит, електропровідність.